

Electronic properties of random alloys: Special quasirandom structures

S.-H. Wei, L. G. Ferreira, James E. Bernard, and Alex Zunger
Solar Energy Research Institute, Golden, Colorado 80401

(Received 16 April 1990)

Structural models needed in calculations of properties of substitutionally random $A_{1-x}B_x$ alloys are usually constructed by randomly occupying each of the N sites of a periodic cell by A or B . We show that it is possible to design “special quasirandom structures” (SQS’s) that mimic for small N (even $N=8$) the first few, physically most relevant radial correlation functions of an infinite, perfectly random structure far better than the standard technique does. These SQS’s are shown to be short-period superlattices of 4–16 atoms/cell whose layers are stacked in rather nonstandard orientations (e.g., [113], [331], and [115]). Since these SQS’s mimic well the local atomic structure of the random alloy, their electronic properties, calculable via first-principles techniques, provide a representation of the electronic structure of the alloy. We demonstrate the usefulness of these SQS’s by applying them to semiconductor alloys. We calculate their electronic structure, total energy, and equilibrium geometry, and compare the results to experimental data.

I. INTRODUCTION: NONSTRUCTURAL THEORIES OF RANDOM ALLOYS

Early experiments^{1–7} on bulk isovalent semiconductor alloys $A_{1-x}B_x$ revealed that many of their properties represent a simple and continuous compositional (x) interpolation between the properties of the end-point solids A and B . For example: (i) alloy lattice parameters are nearly linear with x (Vegard’s rule⁸); (ii) unlike glasses, amorphous semiconductors, or heavily doped systems, isovalent semiconductor alloys generally do not exhibit any substantial gap or “tail” states; (iii) diffraction patterns of melt-grown semiconductor alloys have the same symmetry as those of the constituent solids (with no extra spots); (iv) absorption and reflectance spectra are rather sharp, showing only small alloy broadening near the edge transitions; the λ th transition energy $\epsilon_\lambda(x)$ shifts rigidly with composition as

$$\epsilon_\lambda(x) = [(1-x)\epsilon_\lambda(A) + x\epsilon_\lambda(B)] - b_\lambda x(1-x), \quad (1.1)$$

where b_λ (the “bowing coefficient”) is nearly composition independent; (v) the principal Raman peaks shift smoothly with composition; and (vi) the mixing enthalpy $\Delta H(x)$ is small, positive, and has a simple composition dependence $\Omega x(1-x)$ with nearly constant “interaction parameter” Ω , as expected from a regular solution model.

It is therefore understandable that early electronic structure theories described such alloys in terms of weak, symmetry-preserving perturbations about the end-point constituents. Indeed, these theories are *nonstructural*, in that they consider only the average occupations by $\langle A \rangle$ or $\langle B \rangle$ of lattice sites (i.e., retaining the topology), removing, however, the informational content associated with the *geometrical arrangements* of atoms around sites. Such is the “virtual-crystal approximation”⁹ (VCA), where the alloy is assumed to have a single, $\langle AB \rangle$ averaged type of atom, or the “site-coherent-potential approximation”¹⁰ (SCPA), where the potential is modified rela-

tive to the VCA only on *sites*, hence all A ’s and separately all B ’s are assumed equivalent and each is embedded in a *uniform* medium.

The VCA is limited to valence-only electronic structure methods (since core states remain distinct in the alloy and hence are not amenable to averaging). It has been applied to a wide range of systems using simple valence-only Hamiltonians such as the pseudopotential method,^{11–18} the dielectric two-band model,^{19–21} and the empirical tight-binding model.^{22–25} The SCPA is presently limited to electronic structure methods using atom-anchored representations (where the potential or its matrix elements can be associated with specific atomic sites). It has been applied within empirical pseudopotentials,^{26–28} $\mathbf{k} \cdot \mathbf{p}$ perturbation methods,^{29,30} tight-binding,^{31,32} bond-orbital,^{33,34} and Korringa-Kohn-Rostocker^{35,36} (KKR) methods to a wide range of alloys. Both the VCA and the SCPA are able to capture effects associated with symmetry-preserving, uniform volume changes (e.g., the “volume deformation” contribution³⁷ to the optical bowing b_λ). The SCPA can also capture effects associated with the existence in the alloy of statistical distribution of sites (hence, alloy broadening of absorption bands^{38,39}) and the disparity between the two, chemically inequivalent sites $A \neq B$ (hence, different core-level shifts⁴⁰ for A and B). The principal simplification in these methods lies in the association of average alloy properties with those of “effective atoms” on *sites*, not bonds or tetrahedra, etc. Hence, since non-structural models are based on an effective Hamiltonian with the full symmetry of the parent compounds, they describe pseudobinary (AC)_{1-x}(BC)_x = $A_{1-x}B_xC$ alloys as having single types of “average” A , B , and C atoms. In fourfold coordinated tetrahedral alloys, for example, each C is assumed by these theories to have four *identical* “medium nearest neighbors,” a configuration denoted CX_4 ; the point symmetry around C is then T_d [disorder in this common sublattice could, however, be introduced by using in coherent potential approximation (CPA)]

different diagonal energies for different *C* atoms]. In actuality, possible nearest-neighbor arrangements around *C* include CA_3B and CAB_3 (C_{3v} symmetry), CA_2B_2 (D_{2d} symmetry) as well as CA_4 and CB_4 (T_d symmetry); more configurations occur when one proceeds to more distant shells. Each of these CA_nB_{4-n} ($0 \leq n \leq 4$) clusters could contribute differently to a given physical property. For example, crystal-field splitting, the *A-B* charge transfer, and the positional relaxation of the *C* atom are allowed in C_{3v} and D_{2d} structures, but vanish by symmetry in the T_d structure where all atoms around *C* are identical. Furthermore, some optical transitions that are allowed in the lower-symmetry (CA_3B , CA_2B_2 , and CAB_3) structures become forbidden in the higher-symmetry (CX_4) structure, e.g., zinc-blende $\Gamma \rightarrow X$ transitions carry a zero oscillator strength in VCA, but can have finite oscillator strength in models that distinguish the *A* site from the *B* site. Reference 30 quotes such theoretical and experimental examples. Simple molecular analogs that illustrate the effect of such symmetry lowering on physical properties include the molecules CH_nF_{4-n} , $SiCl_nI_{4-n}$, and $SnCl_nBr_{4-n}$; the qualitative variations with *n* of their vibrational, optical, and chemical-shift characteristics have been studied in detail.⁴¹ Nonstructural alloy theories do not represent such distinct effects associated with symmetry lowering: since only single *sites* are recognized by the theory, all geometries are averaged out to produce a single, *C*-centered configuration CX_4 with the higher, T_d symmetry of the parent compounds. Hence the averaging process projects out only the high-symmetry component of the property in question. Nonstructural theories are, therefore, appropriate only to the extent that the pertinent physical properties are insensitive to symmetry-lowering fluctuations arising from the distinct microscopic structure beyond the central site.

While various empirical parametrizations often used in the VCA (Refs. 11–25) and the SCPA (Refs. 26–34) could help in producing agreement with a set of measured data, the above analysis suggests that one should examine the evidence for the influence of such structural fluctuations beyond sites. Consider, for example, the following.

(i) Extended x-ray-absorption fine-structure (EXAFS) experiments on nearly *random* (melt-grown, bulk) $A_{1-x}B_xC$ semiconductor alloys^{42–46} show that the actual (alloy-averaged) local structure about *C* is not tetrahedral, despite the fact that the constituents *AC* and *BC* are perfectly tetrahedral. Indeed, the alloy-averaged bond lengths around *C* show $R(A-C) \neq R(B-C)$; the next-nearest-neighbor bonds show $R(A-A) \neq R(A-B) \neq R(B-B)$, and the bond angles, e.g., $\theta(A-C-B)$ are nontetrahedral. (These *local* distortions do not necessarily lead to new diffraction spots.) The magnitude of these deviations can be significant in lattice-mismatched III-V and II-VI alloys. These distortions are *not* associated with (topological) short-range order—they persist in high-growth-temperature samples,⁴² and are quantitatively explainable even in terms of models of perfectly *random networks*.^{43,47–50} They simply reflect the lower symmetry associated with *locally strain-minimizing arrangements*^{47,48} of atoms of dissimilar sizes, much like the situation in CX_nY_{4-n} molecules.⁴¹

(ii) $A_{1-x}B_xC$ alloys whose constituents are size mismatched can be ferroelectric, e.g.,⁵¹ $Cd_{1-x}Zn_xTe$. Clearly, the site symmetry cannot be T_d .

Given that the alloy structure has lower global symmetry than that assumed in nonstructural theories, one wonders next how such fluctuations affect the electronic, optical, and thermodynamic properties of the alloy. The evidence here is theoretical, as follows.

(iii) The mixing enthalpies⁵² of a number of semiconductor alloys have been calculated both with and without structural relaxation.^{52–55} Notwithstanding symmetry-preserving hydrostatic volume changes, the local relaxation of the common sublattice *C* in $A_{1-x}B_xC$ by itself lowered the excess enthalpy by up to⁵⁴ 80%; relaxation of the mixed, *A-B* sublattice lowered it further by up to⁵⁵ 20%. These relaxations lower the miscibility gap temperature of semiconductor alloys⁵⁵ and the order-disorder temperature in⁵⁶ $Cu_{1-x}Au_x$ by hundreds of degrees K.

(iv) The optical bowing coefficient *b* [Eq. (1.1)] of the direct band gap was modeled³⁷ for a number of semiconductor alloys at $x = \frac{1}{2}$ using the CuAu-I structure both with and without relaxation of the cell-internal atomic positions (distinct from *volume* deformations). Model calculations showed that the ratio b_s/b of the contribution of the structural (*s*) relaxation piece b_s to the total bowing *b* is

$$b_s/b = \begin{cases} 0.94/1.23=0.76 & \text{for } GaAs_{0.5}Sb_{0.5}, \\ 0.45/0.39=1.15 & \text{for } ZnS_{0.5}Se_{0.5}, \\ 1.32/1.96=0.67 & \text{for } ZnSe_{0.5}Te_{0.5}, \\ 2.68/3.83=0.70 & \text{for } ZnS_{0.5}Te_{0.5}, \\ 0.23/1.08=0.21 & \text{for } Ga_{0.5}In_{0.5}P. \end{cases} \quad (1.2)$$

Clearly, geometrical relaxations absent in nonstructural models such as VCA and SCPA not only lower the total energy but also control optical bowing in size-mismatched alloys. In the rare cases of size-matched alloys ($Al_{1-x}Ga_xAs$ and $Hg_{1-x}Cd_xTe$), one expects to have but small structural relaxation,³⁷ hence nonstructural theories can apply.

The lowering of the site symmetry in isovalent alloys relative to the constituents can also introduce charge transfer about the *C* atom bonded to A_nB_{4-n} . Interestingly, there is evidence that such effects survive alloy averaging and result in the existence in the random alloy of *distinctly* different *C* atoms. The evidence here includes the following.

(v) Nuclear-magnetic-resonance (NMR) chemical shifts $\sigma_C(A_nB_{4-n})$ of the common atom *C* are resolvable into five components ($0 \leq n \leq 4$), e.g., in⁵⁷ $Cd_{1-x}Zn_xTe$. These reflect distinct contributions by the five local atomic arrangements of the *A* and *B* nearest-neighbor atoms to *C*. Similar results have been obtained for⁵⁸ $Hg_{1-x}Cd_xTe$.

(vi) The vibrational spectra of homogeneous random alloys are interpretable^{59,60} in terms of a superposition of frequencies characteristic of the *distinct* local clusters. Furthermore, such alloys can exhibit “no-phonon indirect

transitions,"^{4,61} which can be thought of as folded (pseudodirect) excitations, and can be described also by the SCPA approach.³⁰

Some of these manifestations of the effects of the microscopic atomic structure beyond sites can be partially addressed by refinements of nonstructural alloy theories, e.g., by introducing charge-transfer effects²⁸ into the VCA, adjusting the nearest-neighbor ("hopping") Hamiltonian matrix elements (off-diagonal disorder^{33,62}), by enlarging the SCPA cell to include effectively more atoms (molecular CPA),⁶³ by using the "traveling-cluster approximation"⁶⁴ and its extensions,⁶⁵ or through the "next-neighbor CPA."⁶⁶ The evidence that, even in nearly perfectly random semiconductor alloys, many of the fundamental physical properties are *controlled* by events that are not describable in terms of high-symmetry sites alone suggests to us, however, that an *explicit* structural theory of alloys is in order. Indeed, one of the significant realizations to emerge from recent first-principles electronic structure calculations of crystals, impurities, and surfaces^{67–69} is that electronic properties sensitively reflect the details of the microscopic atomic arrangements, including small changes in atomic positions ("relaxation"). Yet, most alloy theories to date are both nonstructural and based on simple, empirical, electronic Hamiltonians.

We introduce here a different conceptual framework for describing the properties of random alloys.⁷⁰ We ask whether one can construct a periodic unit cell, occupying its M lattice sites by A and B in a single, "special" configuration such that the structure as a whole closely resembles the *configuration average* of an infinite, perfectly random $A_{1-x}B_x$ alloy. To the extent that this is achievable with "supercells" with a sufficiently small number M of atoms per cell (such that first-principles electronic structure theories, currently limited to $M \sim 50$ atoms, can be used), we have a workable *structural theory* of alloys. If the *structure* of such a solid closely resembles (by construction) that of the random alloy, so would its total energy, charge density, density of states, and other electronic properties. We quantify the extent to which a single, finite M arrangement of A 's and B 's mimics the perfectly random infinite alloy through its calculated *structural correlation functions*, familiar from statistical lattice models.^{71–76} We then seek periodic arrangements of A 's and B 's on an M -site unit cell that will directly minimize, for each M , the difference between its structural correlation functions and those of the perfectly random infinite alloy [known analytically, see Eq. (2.8) below]. Describing random alloys by *periodic* structures will clearly introduce spurious correlations beyond a certain distance ("periodicity errors"). However, many physical properties of solids are characterized by microscopic length scales that can be ordered according to size to form a hierarchy. For example, interactions between distant neighbors generally contribute less to the total energy than do interactions between close neighbors.^{55,76} We hence guide our construction of "special quasirandom structures" by the principle of close reproduction of the perfectly random network for the first few coordination shells around a given site, deferring "periodicity errors"

to more distant neighbors. To the extent that the relevant physical property is decided primarily by the "local" structure (see below), this will provide an adequate representation. This approach has an obvious resemblance to the principle guiding the selection of "special k points" for Brillouin zone integration.⁷⁷ By construction, it is not intended to reproduce properties reflecting mostly the long-range order, e.g., diffraction scattering factors.

We show here that by *selective* occupation of the M lattice sites by A and B atoms we can construct *special* periodic "quasirandom structures" that mimic, for finite M the first few, physically most relevant correlation functions of an infinite substitutional random alloy far more closely than does the standard approach of occupying each of the M sites randomly by A or B . While both approaches produce the same results for $M \rightarrow \infty$, the present approach produces excellent approximations already for $M = O(10)$; hence it affords application of accurate electronic structure methods⁶⁷ for calculating structural, optical, and thermodynamical properties of random alloys. This is illustrated here for a number of semiconductor alloys.

Introduction of this concept requires the establishment of some of the basic ideas of statistical lattice models of multisite Ising Hamiltonians. Section II introduces these concepts and formulates the associated notation in such a way that our basic idea (Sec. III) and its relationship to previous work become obvious. Section IV describes the application of our "special quasirandom structures" (SQS) to the study of the electronic and thermodynamic properties of eight semiconductor alloys using the first-principles local-density formalism.^{78–83}

II. STRUCTURAL THEORIES OF ALLOYS

A. Direct sampling methods \Rightarrow with ≈ 2.1 unfavorable to study with $\approx 10^N$ sites, and other methods finding the average.

A binary $A_{1-x}B_x$ substitutional alloy with a lattice of N sites can occur in 2^N possible atomic arrangements, denoted as "configurations" σ . Each configuration exhibits certain physical properties (e.g., total energy, band gap, density of states, etc.) denoted symbolically by $E(\sigma)$. The measurable property $\langle E \rangle$ represents an ensemble average⁷⁴ over all 2^N configurations

$$\langle E \rangle = \sum_{\sigma}^{2^N} \rho(\sigma) E(\sigma), \quad \text{Average properties of a set of configurations} \quad (2.1)$$

where the density matrix $\rho(\sigma)$ denotes the probability to find configuration σ in an ensemble of systems. The obvious difficulty with structural theories of alloys based on Eq. (2.1) lies in the need to relax, then average over a large number of configurations. In practice, one proceeds by either (i) selecting a smaller number of "representative" configurations ("importance sampling techniques"), such as in the Monte Carlo method,⁸⁴ or by (ii) using a single, sufficiently large configuration. While by the principle of spatial ergodicity, all possible finite environments are realized in a single, $N \rightarrow \infty$ sample, in practice far smaller "supercells" have been used. Recent examples include the 64-atom $\text{Al}_{16}\text{Ga}_{16}\text{As}_{32}$ cell used by Lee, By-

lander, and Kleinman,⁸⁵ the ~1000 atom cell of $\text{Pb}_{1-x}\text{Sr}_x\text{S}$ used by Davis,⁸⁶ the ~2000 atom model of $(\text{GaAs})_{1-x}\text{Ge}_{2x}$ used by Davis and Holloway,⁸⁷ and earlier model calculations by Alben *et al.*,⁸⁸ with 8000–10 000 atoms, and by Henderson and Ortenburger⁸⁹ on disordered 8–12 atom cells of Ge. All but the first example⁸⁵ utilized highly simplified Hamiltonians; current first-principles, self-consistent theories of the electronic degrees of freedom^{67–69} are restricted to $N \lesssim 50$ atoms. This direct sampling approach *explicitly* specifies the alloy structure, and can hence incorporate atomic relaxations. However, it approaches the statistical limit as slowly as $N^{-1/2}$, and therefore involves a rather large number of different configurations (e.g., 10^6 in Monte Carlo⁸⁴) or large cell sizes ($\sim 10^3$ atoms^{86–88}), for which first-principles, self-consistent theories are still impractical.

B. Cluster expansions

Rather than address directly the property $E(\sigma)$ of configuration σ taken as a whole, lattice theories^{71–76} proceed by discretizing each configuration into its component “figures” f , and represent the physical property $E(\sigma)$ in terms of a sum of the elemental properties ε_f of the constituent figures $\{f\}$. A figure⁵⁵ is defined by the number k of atoms located on its vertices ($k=1, 2, 3$ are sites, pairs, triplets, etc.), the order m of neighbor distances separating them ($m=1, 2$ are first, second neighbors, etc.), and by the position l of the figure in the lattice (l includes also its orientation). There are D_f equivalent figures per site. Using the language of Ising models,^{74–76} we assign to each site i in a figure a spin variable \hat{S}_i , which takes the value -1 if the site is occupied by *A* or $+1$ if occupied by *B*. Define as $\Pi_f(l, \sigma)$ the product $\prod_i \hat{S}_i$ of spin variables for figure f positioned in the lattice at location l . A configuration σ is then characterized by the values of its spin products $\Pi_f(l, \sigma)$. A lattice average (denoted by a bar) over all locations l of a figure of type f gives

$$\bar{\Pi}_f(\sigma) = \frac{1}{ND_f} \sum_l \Pi_f(l, \sigma). \quad (2.2)$$

The set $\{\bar{\Pi}_f(\sigma)\}$ provides a compact way of characterizing the type of a structure σ . For example,^{55(a)} the CuAuI ($L1_0$) or the CuPt ($L1_1$) ordered structures have $\bar{\Pi}_f$ values of $-\frac{1}{3}, 1, -\frac{1}{3}, 1$ and $0, -1, 0, 1$ for the pair figures separated by first, second, third, and fourth neighbors ($m=1, 2, 3$, and 4), respectively. More examples are given in Table I of Ref. 55(a).

The discretization of a configuration into a hierarchy of figures affords a corresponding hierarchy of approximations for measurable properties, i.e., the ensemble average over configurations. If $\varepsilon_f(l)$ denotes the contribution of figure f at l to a physical property E , the value of E for configuration σ is given by the weighted superposition

$$E(\sigma) = \sum_{f,l} \Pi_f(l, \sigma) \varepsilon_f(l). \quad (2.3)$$

relating the contribution to Properties from a single figure. Figures are useful to arrange a hierarchical system of properties

Since $\{\Pi_f(l)\}$ forms a complete set of *orthogonal* functions⁷⁴

$$\sum_{\sigma} \Pi_f(l, \sigma) \Pi_{f'}(l', \sigma) = 2^N \delta_{f,f'} \delta_{l,l'} \quad (2.4)$$

the “effective cluster property” is given from Eqs. (2.3) and (2.4) as

$$\varepsilon_f(l) = 2^{-N} \sum_{\sigma} \Pi_f(l, \sigma) E(\sigma). \quad (2.5)$$

Since $E(\sigma)$ depends on composition, ε_f does too.

Not that $\varepsilon_f(l)$ does not depend on l , since Eq. (2.5) indicates that $\varepsilon_f = \varepsilon_f(l)$ has the full symmetry of the crystal. Using Eq. (2.2), the cluster expansion of Eq. (2.3) can be written as

$$E(\sigma) = N \sum_f D_f \bar{\Pi}_f(\sigma) \varepsilon_f. \quad (2.6)$$

The ensemble average (denoted by the angular brackets) is

$$\langle E \rangle = N \sum_f D_f \langle \bar{\Pi}_f \rangle \varepsilon_f. \quad (2.7)$$

The basic problem of a *direct* sampling of $E(\sigma)$ over 2^N terms [Eq. (2.1)] is hence transformed into the problem of Eqs. (2.5) and (2.7) where one needs to calculate the effective *cluster* properties ε_f and sum over *all* types of figures. Note that the expansions in Eqs. (2.2)–(2.7) are rigorous⁷⁴ as long as the sum is not truncated. For a perfectly random (R) infinite alloy, the correlation functions are known in advance; they are

$$\bar{\Pi}_{k,m}(R) = \langle \bar{\Pi}_{k,m} \rangle_R = (2x-1)^k, \quad (2.8)$$

where f has been replaced by the equivalent indices (k, m) ; at $x=\frac{1}{2}$ they vanish to all orders, except $\langle \bar{\Pi}_{0,1} \rangle_R = 1$ (see also the Appendix).

While Eqs. (2.2)–(2.7) are rigorous, practical applications of lattice models assume that the cluster expansion of Eq. (2.6) for the relevant observable E is fairly rapidly convergent, so that only a few terms need to be kept. Since this assumption is not inherent in the lattice theory itself, we will examine its validity by constructing specific physical models for the property E . Most lattice models proceed, however, under this assumption to find tractable methods for evaluating the effective cluster property ε_f in Eq. (2.5). Once this is known, the generalized Ising model of Eq. (2.6) can be solved (usually, approximately) to find the ensemble average of Eq. (2.7).

C. Calculation of effective cluster properties ε_f

Lattice theories are traditionally applied to the case where E is the excess total energy, and $\varepsilon_{k,m}$ is the many-body interaction energies [although the expansion (2.6) is applicable to other physical properties as well]. In the vast majority of applications (e.g., see reviews in Refs. 75 and 76), the interaction energies were not calculated, but were assumed to have fixed numerical values used to qualitatively describe alloy phase stability in terms of the postulated values of ε_f . However, $\{\varepsilon_f\}$ can also be calcu-

lated from a microscopic theory of electronic interactions, as discussed below.

1. Direct configurational average

In the "direct configurational average" method^{90–94} one evaluates ϵ_f directly from Eq. (2.5), truncating the sum to a small number of configurations σ (or equivalently, to small N). For example, Lambin and Gaspard⁹⁰ applied this method to $E(\sigma) = \mu_p(\sigma)$, i.e., the p th-order moment of the local density of states, and Berera *et al.*^{92(a)} and Dreyssse *et al.*^{92(b)} have used the direct configurational average method, where the property $E(\sigma)$ was the *integrated* density of states

$$E(\sigma) = \int_{-\infty}^{\epsilon_F} \epsilon n(\epsilon, \sigma) d\epsilon ,$$

and ϵ_F is the Fermi energy. Restricting $f = (k, m)$ to nearest-neighbor pairs ($k = 2, m = 1$), they find the effective pair interactions $\epsilon_{2,1}$; the expansion converged after 10–20 configurations were included.

2. Superposition of periodic structures

To the extent that the basic cluster expansion of Eq. (2.6) converges regularly and rapidly with respect to the figures $\{f\}$, one can use *any* sufficiently large set of configurations $\{\sigma\}$ in Eq. (2.6) to evaluate the effective cluster properties⁵⁵ $\{\epsilon_f\}$. Conversely, nonunique values of $\{\epsilon_f\}$ obtained from two different sets of configurations $\{\sigma\}$ and $\{\sigma'\}$ of comparable sizes testify to the importance of interactions beyond the truncation limit set in the choice of σ and σ' . This suggests that one can (i) establish the largest figure F to be retained in the cluster expansion of Eq. (2.6), (ii) select a *convenient* set of configurations $\{\sigma\}$ from which ϵ_f for $f \leq F$ can be obtained, and (iii) examine convergence by using $\{\epsilon_f\}$ to predict *other* structures; if this fails, F is increased until transferability is established. This approach was carried out by Ferreira, Wei, and Zunger^{55(a)} and Wei, Ferreira, and Zunger.^{55(b)} Here, one specializes the cluster expansion to a set of N_s *periodic structures* $\{\sigma\} = \{s\}$

$$E(s) = N \sum_f^F D_f \bar{\Pi}_f(s) \epsilon_f , \quad (2.9)$$

and obtains the effective cluster properties through matrix inversion

$$\epsilon_f = \frac{1}{ND_f} \sum_s^{N_s} [\bar{\Pi}_f(s)]^{-1} E(s) , \quad (2.10)$$

as shown by Connolly and Williams.⁹⁵ Again, since $E(s)$ depends on composition [e.g., through the volume $V(X)$ of s], so does $\epsilon_f = \epsilon_f[V(X)]$. Carlsson^{55(c)} and we^{55(b)} have recently shown that folding of long-range interactions into Eq. (2.10) introduces an additional *explicit* composition dependence into ϵ_f . Note that the rigorous proof⁷⁴ of Eq. (2.6) does not require that $\{\epsilon_f\}$ depend on composition. However, an accelerated convergence of the truncated sum can be achieved by introducing such a composition dependence.⁵⁵ The situation here is analogous to the expansion of a wave function in a set of basis

orbitals: these need not be individually unique, but they combine to reproduce a unique wave function. This expansion can hence be carried out using a linear, energy-independent basis set (analogous to composition-independent ϵ_f 's); the convergence of the wave-function expansion, can, however, be accelerated by using an energy-dependent basis set.

Two distinct convergence problems are encountered in Eqs. (2.9) and (2.10): that of truncating the sum over figures in Eq. (2.9) and that associated with using a limited set of structures in Eq. (2.10). Assuming that these sums are sufficiently well converged, the configurational property $E(\sigma)$ for *any* σ is then given as a superposition of the properties $E(s)$ of a set of N_s *periodic structures*

$$E(\sigma) = \sum_s^{N_s} \xi_s(\sigma) E(s) , \quad (2.11)$$

where the weights are given by the matrix product

$$\xi_s(\sigma) = \sum_f^F [\bar{\Pi}_f(s)]^{-1} \bar{\Pi}_f(\sigma) . \quad (2.12)$$

The ensemble average for phase γ is

$$\langle E \rangle_\gamma = \sum_s P_s(x, T) E(s) , \quad (2.13)$$

where $P_s(x, T) = \langle \xi_s \rangle_\gamma$ is the weight of s in phase γ at (x, T) .

One might at first wonder if this procedure of describing the excess energy $\langle E \rangle$ of an alloy in an arbitrary configuration (say, *random*) by constructs obtained from *ordered* structures $\{s\}$ is likely to be valid, given the often-noted differences in the electronic structure of random and ordered alloys of the same composition. However, inspection of Eqs. (2.9)–(2.13) reveals that the only real question here is one of *convergence* with respect to figures and structures. This question can be handled quantitatively by actual convergence tests (see below).

The application of this method proceeds by (i) selection of a set of figures $\{f\}$ and a set of N_s periodic structures $\{s\}$; (ii) calculation of $\{E(s, V)\}$ (e.g., excess total energies, band gaps, density of states) for each of the fully relaxed N_s structures as a function of the external volume V . This can be done,⁵⁵ e.g., by the linear augmented plane wave (LAPW) method⁸² or by the plane-wave non-local pseudopotential method;⁷⁹ (iii) inversion of the set $\{E(s, V)\}$ to obtain a set of N_s functions $\{\epsilon_f(V)\}$ from Eq. (2.10). (iv) Examination of transferability: this set is used in Eq. (2.9) to predict the quantities $E(s', V)$ for *another* set of structures $\{s'\} \neq \{s\}$; comparison with the directly calculated $E(s', V)$, e.g., using the LAPW or pseudopotential methods establishes truncation errors in the expansions of Eqs. (2.9) and (2.10). The maximum figure F is then increased until the errors are lowered below a prescribed tolerance; (for zinc-blende-based systems, F had to be extended⁵⁵ up to fourth neighbors pairs and four-body terms). (v) The set $\{\epsilon_f(V)\}$ can then be used in Eq. (2.7); solution of this generalized Ising Hamiltonian by Monte Carlo⁸⁴ or cluster-variation^{71–73} methods (CVM) produces the desired averages $\langle E \rangle$ (this is practiced only if the set of interactions is not too large).

The basic advantage of this approach lies in its ability

to describe disordered alloys with terms (and accuracy) equivalent to those with which state-of-the-art methods address simple periodic crystals. Indeed, since we are dealing with periodic crystals $\{s\}$, their physical properties E can be calculated by (first-principles, self-consistent) band-structure techniques,^{67–69,79–82} avoiding the simplified empirical methods used in previous applications of either the direct configurational average,^{86–89} the VCA (Refs. 11–25), or the SCPA.^{26–34} Furthermore, this approach is clearly “structural” in that it represents the alloy as a collection of different local environments, permitting each to relax so that the cluster properties $\{\varepsilon_f\}$ include the effect of such relaxations. Hence, while the ensemble average in (2.13) reflects the symmetry of the pertinent phase γ (e.g., random), the individual cluster contributions ε_f reflect the *local* symmetry, including such relaxations permitted by that symmetry. The same basic thought (but with a different interpretation of the weights ξ_s) has been sketched earlier by Butler and Kohn,⁹⁶ who referred to Eq. (2.11) as the method of superposition of “periodically continued neighborhoods.” It obviously applies to physical quantities E that are “local” in the sense that the radius of influence of relevant perturbations must be smaller than the cell radius. The current formulation shows how this method can be naturally developed from a general cluster expansion, where a choice of periodic structures corresponds to a particular truncation of the expansion of f ’s. The convergence is then examined systematically by the transferability condition.

The method of superposition of periodic structures has been used by a number of authors, *restricting F to a nearest-neighbor figure*. Within this approximation, there are only five nonequivalent values of $f=(k,m)$, i.e., $m=1$ and $k=0, 1, 2, 3$, and 4 ; the maximum figure F is the A_nB_{4-n} tetrahedron with $0 \leq n \leq 4$; the $N_s=5$ structures are obtained by superposition of these figures. For fcc alloys, these can be conveniently selected for $n=0, 1, 2, 3$, and 4 as B_4 (fcc), AB_3 (Cu₃Au-type), A_2B_2 (CuAuI-type), A_3B (Cu₃Au-type), and A_4 (fcc), respectively. Applications of this nearest-neighbor model to E equal to total energy include the pioneering work of Connolly and Williams⁹⁵ and Terakura *et al.*⁹⁷ on transition-metal alloys, that of Srivastava, Martins, and Zunger⁴⁸ and Mbaye and co-workers^{52–54} on semiconductor alloys; the work of Wei *et al.*⁵⁶ on noble-metal alloys and that of Mbaye, Wood, and Zunger^{54(a)} and Wood and Zunger^{54(b)} on epitaxial systems. All of these applications were carried out with first-principles electronic structure techniques. Applications to E equal to band gaps include the work of Bernard and Zunger^{37(a)} on II-VI alloys, and Wei and Zunger^{37(b)} and Ling and Miller⁹⁸ on III-V alloys. Applications to E equal to spin-orbit splittings were carried out by Chadi²⁵ and by Wei and Zunger.⁹⁹ Finally, applications to E equal to bond lengths were carried out by Balzarotti *et al.*,⁴³ Letardi, Motta, and Balzarotti,⁴⁹ Ichimura and Sasaki,⁵⁰ Martins and Zunger,⁴⁷ and Wei and Zunger.^{37(b)}

Extension of the superposition of periodic structures approach of Eqs. (2.9)–(2.13) to include a *converged* set of figures (e.g., up to fourth neighbors in fcc systems) was

presented by Ferreira, Wei, and Zunger^{55(a)} and by Wei, Ferreira, and Zunger^{55(b)} on different II-VI and III-V alloys.

Like any sampling method, the superposition of periodic structures approach is effective only as long as the variance of the pertinent physical property is sufficiently smaller than the mean; otherwise, a large number of structures needs to be included. In turn, this variance reflects the dependence of the property on the microscopic structure through its correlation functions, i.e., $E(\sigma)=E(\{\langle \bar{\Pi}_f \rangle\})$. While the choice E being the total energy and σ the interaction energies representing quantities that are integrated both over the cell volume and the Brillouin zone, appears to exhibit rather fast convergence in cluster expansion,⁵⁵ it is possible that other properties, such as distinct one-electron band gaps, could depend more sensitively on $\{\langle \bar{\Pi}_f \rangle\}$. (One can certainly imagine some configurations leading to an insulating band gap, yet others, for the same global composition, leading to a metal.) This led us to consider the possibility of designing *single*, “special” structures s , whose correlation functions $\{\langle \bar{\Pi}_f(s) \rangle\}$ closely reproduce the *ensemble average* $\langle \bar{\Pi}_f \rangle_R$ for a random (R) alloy. The development of this idea is described in the following section.

D. Representative structures

The standard approach for simulating the properties of a random alloy through a finite, N -atoms/cell representation of Eqs. (2.7) and (2.8) (e.g., see Refs. 85–90) assumes that each site should be individually occupied at random by A or B . One then seeks a *single* configuration, with a sufficiently large N , that can be used as a “representative structure.” While for $x=\frac{1}{2}$ the average $\langle \bar{\Pi}_{k,m}(N) \rangle$, taken over a large number of such attempts, is near zero even for finite N [as it should be in a random alloy, Eq. (2.8)], the variance about the average is not. This means that a *single* configuration selected at random from this ensemble might contain errors, measured on average by this variance. The extent to which this approach is likely to produce a single finite N atom/cell structure that, as a whole, approaches randomness can be measured by the standard deviations $\eta_{k,m}(N)=|\langle \bar{\Pi}_{k,m}^2 \rangle|^{1/2}$. For an isolated lattice with N sites we find that $\eta_{k,m}(N)=(D_{k,m}N)^{-1/2}$ (see also the Appendix). Application of this procedure to *periodic* structures with values of N typical of the sizes for which first-principles electronic structure calculations are practical, could produce even larger errors. This is seen in Table I in the columns headed “standard deviation in $\bar{\Pi}_{2,m}$ ” which gives for $x=\frac{1}{2}$ the standard deviation $\eta_{2,m}(N)$ obtained by randomly occupying N fcc sites of the unit cell in a sufficiently large number of ways so that converged statistics are obtained. Comparison with $(D_{2,m}N)^{-1/2}$ reveals larger periodicity errors in this site-by-site occupation method; e.g., for $N=32$, the ratios between the standard deviations of Table I and $(D_{2,m}N)^{-1/2}$ are 1.43, 1.45, and 2.03 for the second-, third-, and fourth-neighbor correlations, respectively. Furthermore, in some cases periodicity errors can lead to average correlation function values of ~ 1 rather

Points to the simplifications of studies with
Ab initio methods since we use periodic structures

Super relevant section on why the old methods fail in terms of variance and standard deviation. Particularly in the relevance of N .

than zero (denoted in Table I as “PE”); these occur at rather short distances from the origin for small N . Clearly, this standard method for creating periodic, quasirandom structures approaches the statistical limits only at impractically large values of ^{100}N .

III. SPECIAL QUASIRANDOM STRUCTURES

A. The basic idea

Instead of attempting to approach the random correlation functions $\{\bar{\Pi}_{k,m}(R)\}$ by *statistical* means, we will instead design a *single* “special” N -atom per cell periodic structure whose *distinct* correlation functions $\bar{\Pi}_{k,m}(s)$ best match the *ensemble-averaged* $\langle \bar{\Pi}_{k,m} \rangle$ of the random alloy [Eq. (2.8)]. The cluster expansion of Eqs. (2.3)–(2.8) shows that the amount by which the property $E(\sigma=s)$ of a *given* structure s fails to reproduce the ensemble average $\langle E \rangle$ of the perfectly random alloy can be represented in terms of a *hierarchy* of figures

$$\langle E \rangle - E(s) = \sum'_{k,m} D_{k,m} [(2x-1)^k - \bar{\Pi}_{k,m}(s)] \varepsilon_{k,m}, \quad (3.1)$$

where the prime denotes omission of $k=0$ and 1 terms, which are common to both R and s . In turn, the contribution $\varepsilon_{k,m}$ to the property E is expected to fall off with the size of the figure. Indeed, in disordered systems the physical characteristic E at point \mathbf{R} depends primarily on the environment inside a neighborhood $|\mathbf{R}-\mathbf{R}'| < L$; the effect of more distant neighbors falls off *exponentially*⁹⁶ with $|\mathbf{R}-\mathbf{R}'|/L$, where L is a characteristic length scale of property E (e.g., thermal de Broglie wavelength for scattering, screening length for energy levels). It is hence natural to select the occupations by A and B for the special structures s so that Eq. (3.1) is minimized in a *hierarchical* manner.

In standard lattice theory models,^{71–76} one characterizes *given* structures by their $\{\bar{\Pi}_{k,m}\}$. We will do the inverse: we will first specify a set of correlation functions $\{\bar{\Pi}_{k,m}(s)\}$ that mimics, in a hierarchical manner, $\langle \bar{\Pi}_{k,m} \rangle$ of the random alloy, and then find the structures corresponding to this set $\{\bar{\Pi}_{k,m}(s)\}$. For example, insisting that at $x=\frac{1}{2}$ the physically most important correlation functions—those for the first and second neighbors⁵⁵—have zero errors, gives already for $N=8$ in fcc symmetry at SQS, denoted in Table II as SQS-8. This table gives for $N \leq 14$ the special $x=\frac{1}{2}$ fcc quasirandom structures constrained to have $\bar{\Pi}_{2,1}=0$ and $\bar{\Pi}_{2,2}^2 + \bar{\Pi}_{2,3}^2 + \bar{\Pi}_{2,4}^2 = \text{minimum}$. For each SQS, we give its empirical formula $A_{N/2}B_{N/2}$, the unit cell vectors, and its designation as a superlattice (see caption to Table II). This information completely specifies the crystal structure of each SQS. Figure 1 depicts the structure of three SQS’s.

B. Discussion of the SQS’s

In what follows, we make a number of observations on the SQS’s of Table II. We will focus our discussion on special $x=\frac{1}{2}$ fcc quasirandom structures. Extension to other compositions or symmetries can be easily made.

TABLE I. This table gives, for a range of m th-order pairs in the fcc lattice the absolute value of the pair correlation functions for $x=\frac{1}{2}$, as obtained in special quasirandom structures (SQS) with N atoms. The SQS’s are defined in Table II. The perfectly random infinite lattice has $\langle \bar{\Pi}_{2,m} \rangle_R = 0$ [Eq. (2.8)], hence, deviations from zero in the columns denoted “ $\bar{\Pi}_{2,m}$ for SQS” measure errors. In the columns labeled “standard deviations in $\bar{\Pi}_{2,m}$ ” we give the standard deviations $\eta_{2,m}(N)$ obtained by randomly occupying each of the N sites in a supercell of lattice dimension H by A or B atoms. We use fcc-, bcc-, and sc-like cells. “PE” denotes periodicity errors, i.e., an average correlation function of ~ 1 rather than zero. For isolated lattice $\eta_{2,m}(N) = (ND_{2,m})^{-1/2}$ where $D_{2,m}$ is the degeneracy factor.

mth neighbor	neighbor (units of $a/2$)	$ \bar{\Pi}_{2,m} $ for SQS			Standard deviations in $\bar{\Pi}_{2,m}$			$H=5a$ fcc $N=125$	$H=4a$ bcc $N=128$
		$D_{2,m}$	SQS-4	SQS-8	SQS-14	$H=2a$ fcc $N=8$	$H=2a$ bcc $N=16$	$H=3a$ fcc $N=27$	
First	(110)	6	0	0	0.215	0.102	0.079	0.073	0.051
Second	(200)	3	0.333	0	0.048	0.504	0.206	0.110	0.146
Third	(211)	12	0	0.042	0	0.215	0.102	0.098	0.074
Fourth	(220)	6	0.333	0.083	0.048	PE	0.206	0.079	0.146
Fifth	(310)	12	0	0.083	0	0.215	0.102	0.110	0.073
Sixth	(222)	4	1	0	0.143	0.504	PE	0.098	0.249
Seventh	(321)	24	0	0.125	0.119	0.298	0.146	0.080	0.127
Ninth	(330)	6	0	0	0.095	0.215	0.102	PE	0.073

very relevant for my study.

TABLE II. Special, N -atom fcc quasirandom structures at $x = \frac{1}{2}$. This table gives the empirical formula, the unit cell vectors in units of half the lattice constant, the designation of the SQS- N as a superlattice (SL) and the correlation functions $\bar{\Pi}_{k,m}$. The square brackets next to $\bar{\Pi}_{k,m}$ give the degeneracy factor $D_{k,m}$. The deviations of $\bar{\Pi}_{k,m}$ from zero measures errors relative to the infinite, perfectly random $x = \frac{1}{2}$ alloy. The designation of the superlattice is illustrated as follows: the notation “ $A_2B_3A_2B_1$ ” along [113] for SQS-8 means that one identifies the [113] direction in an fcc cube and occupies along it two planes by A , then three planes by B , then two by A and a single plane by B . Together with the unit cell vectors, this completely defines the structure. For these structures the averaged value of $\bar{\Pi}_{3,m}$ is zero.

Name	SQS-2							
	CuPt	CuAu	SQS-4	SQS-6	SQS-8	SQS-10	SQS-12	SQS-14
Formula	AB	AB	A_2B_2	A_3B_3	A_4B_4	A_5B_5	A_6B_6	A_7B_7
Unit cell	(011)	(110)	(110)	(110)	(110)	(110)	(110)	(211)
vectors	(101)	(110)	(002)	(220)	(211)	(321)	(213)	(202)
	(112)	(002)	(220)	(013)	(224)	(004)	(233)	(141)
SL Sequence	A_1B_1	A_1B_1	A_2B_2	$A_1B_1A_2B_2$	$A_2B_3A_2B_1$	$A_2B_3A_2$ $B_1A_1B_1$	$A_3B_2A_1$ $B_1A_2B_3$	$A_2B_2A_2B_1A_1$ $B_2A_1B_1A_1B_1$
SL Orientation	[111]	[001]	[110]	[331]	[113]	[115]	[335]	[519]
$\bar{\Pi}_{k,m}$:								
$\bar{\Pi}_{2,1}[6]$	0	$-\frac{1}{3}$	0	0	0	0	0	0
$\bar{\Pi}_{2,2}[3]$	-1	1	$-\frac{1}{3}$	$\frac{1}{9}$	0	$\frac{1}{15}$	$-\frac{1}{9}$	$-\frac{1}{21}$
$\bar{\Pi}_{2,3}[12]$	0	$-\frac{1}{3}$	0	$-\frac{1}{3}$	$\frac{1}{24}$	$-\frac{1}{15}$	$-\frac{1}{18}$	0
$\bar{\Pi}_{2,4}[6]$	1	1	$-\frac{1}{3}$	$\frac{1}{9}$	$-\frac{1}{12}$	0	0	$\frac{1}{21}$
$\bar{\Pi}_{2,5}[12]$	0	$-\frac{1}{3}$	0	$\frac{1}{3}$	$\frac{1}{12}$	$-\frac{1}{5}$	0	0
$\bar{\Pi}_{2,6}[4]$	-1	1	1	$-\frac{1}{3}$	0	$\frac{1}{5}$	$\frac{1}{6}$	$-\frac{1}{7}$
$\bar{\Pi}_{4,1}[2]$	-1	1	-1	$\frac{1}{3}$	0	$-\frac{1}{5}$	$-\frac{1}{3}$	$\frac{1}{7}$
$\bar{\Pi}_{4,2}[12]$	0	$-\frac{1}{3}$	0	$-\frac{2}{9}$	$-\frac{1}{6}$	$-\frac{2}{15}$	$-\frac{1}{9}$	$-\frac{1}{21}$

(i) All SQS's studied here are *short-period superlattices*, hence analyzable in terms of conventional superlattice language, e.g., confined states, band folding, and pseudo-direct transitions—see below. (Of course, we do not imply here that an infinite random alloy is a superlattice, but rather that considering only the first few correlation functions, the alloy and the special quasirandom superlattices are nearly indistinguishable structurally; hence, as shown below, also electronically.)

(ii) These SQS's are indeed special in that they approach the correlation functions of the perfectly random alloy much more closely than does the conventional, site-by-site random occupation method for the same N (Table I). For example, SQS-8 is equivalent to $N \rightarrow \infty$ for the first- and second-neighbor correlation functions (as well as for the sixth and ninth), and to $N=64$ for third neighbors. Table I also shows that SQS-14 is equivalent to $N \rightarrow \infty$ for $\bar{\Pi}_{2,1}$, $\bar{\Pi}_{2,3}$, $\bar{\Pi}_{2,5}$ to $N > 128$ for $\bar{\Pi}_{2,2}$; and to $N > 64$ for $\bar{\Pi}_{2,4}$, etc. Note that (by construction) each SQS- N is the best choice out of $N!/(N/2)!(N/2)!$ possible N -atom/cell configurations at $x = \frac{1}{2}$. In this respect, the method of SQS's is analogous to the method of selecting “special \mathbf{k} points” for Brillouin-zone integrations.⁷⁷ There, too, one replaces the exact integral by representative points which minimize the error in suc-

Truncation error

sive shells about an origin. Note further that the only relevant convergence error in the SQS approach is that of truncating the difference cluster expansion of Eq. (3.1), whereas in the method of superposition of periodic structures [Sec. II C 2] we also have the truncation error of expanding ε_f in terms of structures s [Eq. (2.10)].

(iii) A SQS- N of the form $A_{N/2}B_{N/2}$ can comprise $N/2$ crystallographically inequivalent A sites (or B sites). It hence includes a *distribution* of local environments, unlike the VCA. Calculation of electronic or vibrational energy levels of a SQS will hence produce a *distribution* of levels with a finite width. This is analogous to the broadening effect in disordered systems familiar from the CPA.^{26–36} In Sec. IV H we show that this broadening is similar to that seen in the CPA.

(iv) In a perfectly random alloy, a given site (occupied, for example, by A) has an average (over ensemble and lattice sites) $\langle O_m \rangle_R$ neighbors of the opposite type (i.e., B) in shell number m , where (Appendix)

$$\langle O_m \rangle_R = D_m \pm \sqrt{D_m/2}. \quad (3.2)$$

Here, $D_m = Z_m/2$, where Z_m is the number of atoms in the m th shell. Tables IV and V analyze this quantity for SQS-4 and SQS-8. The results are compared to those of

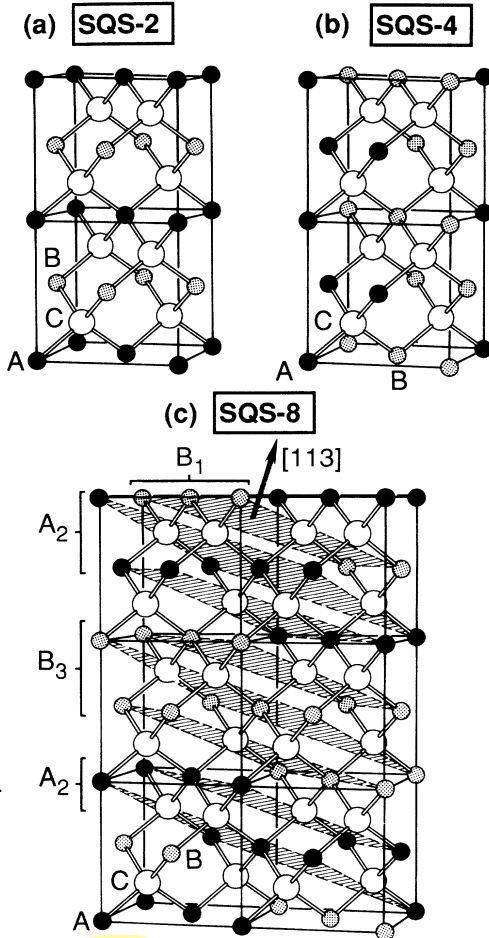


FIG. 1. Crystal structure of three special quasirandom structures. (a) SQS-2 is a (1,1) superlattice in the [001] direction; (b) SQS-4 is a (2,2) superlattice in the [110] direction; and (c) SQS-8 is a (2,3,2,1) superlattice in the [113] direction. The (113) planes are shaded in (c), and the stacking arrangement is indicated.

the perfectly random alloy [Eq. (3.2)]. They show that SQS-8 reproduces the average coordination numbers within the standard deviations of Eq. (3.2).

(v) So far we have constructed SQS's by reproducing the average correlation functions of the perfectly *random*

alloy [Eq. (2.8)]. It is, however, a simple matter to apply the same approach to correlation functions $\langle \Pi_{k,m} \rangle_D$ of *disordered* (D), imperfectly random alloys. These can be obtained, for example, from Monte Carlo or CVM solutions to the Ising problem, e.g., Refs. 52–56.

(vi) For a given external volume $V(x)$, each SQS has some cell-internal atomic coordinates whose values are not restricted by the space group. An equilibrium theory of random alloys hence has to relax these positions to achieve a minimum in the total energy (without symmetry-breaking atom interchanges).

For example, SQS-4—an $(AC)_2(BC)_2$ superlattice along [110]—has the space group $Pmn2_1$ (C_{2v} ,⁷ space group No. 31 in the International Tables for Crystallography) and a primitive orthorhombic unit cell. Its basis vectors are

$$\begin{aligned}\mathbf{a} &= (-\frac{1}{2}, \frac{1}{2}, 0)\eta\mathbf{a}, \\ \mathbf{b} &= (0, 0, 1)\mathbf{a}, \\ \mathbf{c} &= (1, 1, 0)\xi\mathbf{a},\end{aligned}\quad (3.3)$$

where a is the fcc lattice constant. The atoms lie at paired sites with Cartesian coordinates taking the general forms

$$(x_i\xi; x_i\xi; z_i)a \quad (3.4)$$

and

$$(-\frac{1}{4}\eta - x_i\xi; \frac{1}{4}\eta - x_i\xi; \frac{1}{2} + z_i)a,$$

where i ranges from 1 to 4, and the associated atomic identities for $i=1, 2, 3$, and 4 are A, B, C , and C , respectively. Without loss of generality, z_1 can be taken to be zero. For an *unrelaxed*, ideal structure, $\xi=\eta=1$ and the cell-internal parameters take the values $x_1=-\frac{1}{8}$, $x_2=\frac{3}{8}$, $x_3=\frac{1}{8}$, $x_4=-\frac{3}{8}$, $z_2=0$, and $z_3=z_4=\frac{1}{4}$, resulting in the

TABLE III. Number of neighbors of type A in successive shells around atom A in CuAu, CuPt, and the chalcopyrite structures, compared with the corresponding results in a perfectly random $x=\frac{1}{2}$ binary fcc alloy. The number of B atoms is the shell coordination number (CN) minus the number of A atoms. Similar results with B at the center can be obtained by switching A and B in this table.

Structure	Number of A neighbors with atom A at the origin							
	First shell CN=12	Second shell CN=6	Third shell CN=24	Fourth shell CN=12	Fifth shell CN=24	Sixth shell CN=8	Seventh shell CN=48	Ninth shell CN=12
CuAuI	4A	6A	8A	12A	8A	8A	16A	4A
CuPt	6A	0A	12A	12A	12A	0A	24A	6A
Chalcopyrite	4A	4A	16A	4A	8A	0A	32A	4A
Random	6A	3A	12A	6A	12A	4A	24A	6A

TABLE IV. Number of neighbors to a given atom in the SQS-4, the average $\langle O_m \rangle$ of m th shell neighbors of an opposite type, and the corresponding result $\langle O_m \rangle_R$ for the perfectly random alloy [Eq. (3.2)]. The number of B neighbors is the shell coordination number (CN) minus the number of A atoms.

Sublattice	Occup.	Number of A neighbors in SQS-4								
		First shell CN = 12	Second shell CN = 6	Third shell CN = 24	Fourth shell CN = 12	Fifth shell CN = 24	Sixth shell CN = 8	Seventh shell CN = 48	Ninth shell CN = 12	
1	B	$6A$	$4A$	$12A$	$8A$	$12A$	$0A$	$24A$	$6A$	
2	B	$6A$	$4A$	$12A$	$8A$	$12A$	$0A$	$24A$	$6A$	
3	A	$6A$	$2A$	$12A$	$4A$	$12A$	$8A$	$24A$	$6A$	
4	A	$6A$	$2A$	$12A$	$4A$	$12A$	$8A$	$24A$	$6A$	
Random		$6A$	$3A$	$12A$	$6A$	$12A$	$4A$	$24A$	$6A$	
<i>m</i> th-order neighbors of opposite type in SQS-4										
$\langle O_m \rangle$		6 ± 0	4 ± 0	12 ± 0	8 ± 0	12 ± 0	0 ± 0	24 ± 0	6 ± 0	
$\langle O_m \rangle_R$		6 ± 1.7	3 ± 1.2	12 ± 2.4	6 ± 1.7	12 ± 2.4	4 ± 1.4	24 ± 3.5	6 ± 1.7	

atomic positions

- $A(1)$ at $(-\frac{1}{8}, -\frac{1}{8}, 0)a$,
 - $A(2)$ at $(-\frac{1}{8}, \frac{3}{8}, \frac{1}{2})a$,
 - $B(1)$ at $(\frac{3}{8}, \frac{3}{8}, 0)a$,
 - $B(2)$ at $(-\frac{5}{8}, -\frac{1}{8}, \frac{1}{2})a$,
 - $C(1)$ at $(\frac{1}{8}, \frac{1}{8}, \frac{1}{4})a$,
 - $C(2)$ at $(-\frac{3}{8}, \frac{1}{8}, \frac{3}{4})a$,
 - $C(3)$ at $(-\frac{3}{8}, -\frac{3}{8}, \frac{1}{4})a$,
 - $C(4)$ at $(\frac{1}{8}, \frac{5}{8}, \frac{3}{4})a$.
- (3.5)

For the case of a binary fcc alloy (with no common C

sublattice), the space group of the SQS-4 structure is $Pmmn$ (D_{2h}^{13} , space group No. 59 in the International Tables for Crystallography). The atomic positions for the A and B atoms are given by Eq. (3.4) with the added restriction that $z_i = 0$; in this case i takes only the values 1 and 2, since no C atoms are present. The unrelaxed coordinates are the same as those given for the A and B atoms in Eq. (3.5).

The ideal(unrelaxed) SQS-8 structure has the lattice vectors

$$\begin{aligned}\mathbf{a} &= (1, \frac{1}{2}, -\frac{1}{2})a, \\ \mathbf{b} &= (\frac{1}{2}, -\frac{1}{2}, 0)a, \\ \mathbf{c} &= (1, 1, 2)a,\end{aligned}\quad (3.6)$$

belonging to the monoclinic system. The corresponding atomic positions, in Cartesian coordinates, are

TABLE V. Number of neighbors to a given atom in SQS-8, the average $\langle O_m \rangle$ of the m th shell neighbors which are of opposite type, and the corresponding value $\langle O_m \rangle_R$ in the perfectly random alloy [Eq. (3.2)]. The number of B atoms is the shell coordination number (CN) minus the number of A atoms.

Sublattice	Occup.	Number of A neighbors in SQS-8								
		First shell CN = 12	Second shell CN = 6	Third shell CN = 24	Fourth shell CN = 12	Fifth shell CN = 24	Sixth shell CN = 8	Seventh shell CN = 48	Ninth shell CN = 12	
1	B	$7A$	$3A$	$12A$	$6A$	$10A$	$4A$	$24A$	$7A$	
2	B	$5A$	$3A$	$11A$	$7A$	$12A$	$4A$	$30A$	$5A$	
3	A	$2A$	$2A$	$14A$	$6A$	$16A$	$6A$	$24A$	$8A$	
4	B	$5A$	$3A$	$11A$	$7A$	$12A$	$4A$	$30A$	$5A$	
5	B	$7A$	$3A$	$12A$	$6A$	$10A$	$4A$	$24A$	$7A$	
6	A	$7A$	$3A$	$13A$	$5A$	$12A$	$4A$	$18A$	$7A$	
7	A	$8A$	$4A$	$10A$	$6A$	$12A$	$2A$	$24A$	$2A$	
8	A	$7A$	$3A$	$13A$	$5A$	$12A$	$4A$	$18A$	$7A$	
Random		$6A$	$3A$	$12A$	$6A$	$12A$	$4A$	$24A$	$6A$	
<i>m</i> th-order neighbors of opposite type in SQS-8										
$\langle O_m \rangle$		6 ± 1.8	3 ± 0.5	11.5 ± 1.1	6.5 ± 0.5	11 ± 1.4	4 ± 1	27 ± 3	6 ± 1.8	
$\langle O_m \rangle_R$		6 ± 1.7	3 ± 1.2	12 ± 2.4	6 ± 1.7	12 ± 2.4	4 ± 1.4	24 ± 3.5	6 ± 1.7	

$A(1)$,	$(0,0,0)a$	(3.7)
$A(2)$,	$(\frac{1}{2}, \frac{1}{2}, 0)a$	
$A(3)$,	$(\frac{1}{2}, 0, \frac{3}{2})a$	
$A(4)$,	$(0, 0, 2)a$	
$B(1)$,	$(\frac{1}{2}, 0, \frac{1}{2})a$	
$B(2)$,	$(0, 0, 1)a$	
$B(3)$,	$(\frac{1}{2}, \frac{1}{2}, 1)a$	
$B(4)$,	$(\frac{1}{2}, \frac{1}{2}, 2)a$	
$C(1)$,	$(\frac{1}{4}, \frac{1}{4}, \frac{1}{4})a$	
$C(2)$,	$(\frac{3}{4}, \frac{3}{4}, \frac{1}{4})a$	
$C(3)$,	$(\frac{3}{4}, \frac{1}{4}, \frac{3}{4})a$	
$C(4)$,	$(\frac{1}{4}, \frac{1}{4}, \frac{5}{4})a$	
$C(5)$,	$(\frac{3}{4}, \frac{3}{4}, \frac{5}{4})a$	
$C(6)$,	$(\frac{3}{4}, \frac{1}{4}, \frac{7}{4})a$	
$C(7)$,	$(\frac{1}{4}, \frac{1}{4}, \frac{9}{4})a$	
$C(8)$,	$(\frac{3}{4}, \frac{3}{4}, \frac{9}{4})a$	

Note that, due to the changed sign of the $\bar{\Pi}_{3,m}$ correlation functions in $A_2B_3A_2B_1$ and $B_2A_3B_2A_1$ SQS's, these are not equivalent (in practice, they give similar energies, so we average the results).

For a given external volume [e.g., $V(x = \frac{1}{2})$] one needs to relax the symmetry-allowed structural parameters (e.g., x_i and z_i) to achieve a minimum in the total energy. Standard first-principles electronic structure techniques^{78–82} are currently capable of producing rather accurate total energies and equilibrium geometries (through quantum-mechanical force calculations^{79–81}) for periodic structures with the number N of atoms per cell in the range given in Table II.

IV. APPLICATIONS TO SEMICONDUCTOR ALLOYS

A. Electronic Hamiltonian used

Since the SQS's are rather simple periodic (superlattice) structures with a modest number of atoms per unit cell, their equilibrium geometry, total energy, charge densities, and electronic band structures can be calculated from first principles with the same degree of sophistication with which ordinary simple crystals are currently treated. We use the semirelativistic local-density formalism,⁷⁸ treating Coulomb and exchange-correlation⁸³ interelectronic interactions in a self-consistent, mean-field manner. Specifically, we utilize the all-electron (general potential) LAPW (Ref. 82) and the nonlocal pseudopotential method^{79–81} with a plane-wave basis set. This avoids many of the approximations previously used in electronic theory of alloys, such as use of empirical Hamiltonian,^{11–34} first-nearest-neighbor approxima-

tions,^{22–25,31–32} lack of self-consistency,^{11–18,22–28,31–34} spherical approximations to the charge density and potential,^{35,36} neglect of interelectronic terms in the total energy, small basis sets,^{22–25,31–34} and neglect of structural relaxations.^{11–36}

The pseudopotential calculation was undertaken because it affords a more economical calculation of large supercells, e.g., SQS-8 with 16 atoms/cell for an $A_{1-x}B_xC$ alloy. We used Kerker's¹⁰¹ prescription for constructing semirelativistic nonlocal pseudopotentials, a plane-wave basis set cut off of $E1=15$ Ry, and 29 zinc blende-equivalent special \mathbf{k} points⁷⁷ in the irreducible Brillouin zone (this gives 39, 38, and 21 \mathbf{k} points, for SQS-2, SQS-4, and SQS-8, respectively). In our previous study of simple periodic compounds in Ref. 55(b), we used 10 \mathbf{k} points in the pseudopotential calculations, giving slightly different results (see Table VI below). Structural optimizations were carried out using the valence-force-field method;¹⁰² these geometries were then used to perform first-principles total energy and force^{80,81} calculations, verifying thereby the adequacy of the geometry. If necessary, atoms could then be relaxed in an iterative process where these forces, combined with valence-force-field force constants,¹⁰² provide the new atomic geometry, which is then used in a subsequent pseudopotential calculation. The process is terminated when subsequent iterations produce relaxation-induced energy changes of less than 2 meV/4 atoms. We find that this geometry optimization generally produced similar structural parameters (but not total energies) to those obtained in a pure valence-force-field (VFF) optimization. In the LAPW calculations, we hence used VFF as a guide to the geometry. Two special zinc-blende-equivalent \mathbf{k} points⁷⁷ are used in the LAPW calculations. The convergence error in the LAPW and pseudopotential calculations is about 5 meV/4 atoms and slightly larger for II-VI systems. For III-V systems the two methods produce results which differ by this error margin or less, reflecting the differences in residual convergence errors as well as pseudopotential errors of freezing core states.

B. Mixing enthalpy of the random alloy

The mixing enthalpy is defined as the fully optimized energy of the alloy, measured with respect to equivalent amounts of the binary constituents at their bulk equilibrium, i.e.,

$$\Delta H^{(R)}(x) = \langle E(A_x B_{1-x}) \rangle_R - xE(A) - (1-x)E(B). \quad (4.1)$$

Since the central question surrounding the use of the SQS's pertains to the convergence of certain physical properties with figures, we first establish a converged description of $\Delta H^{(R)}$ using the cluster expansion.

1. Using cluster expansions

To establish a reference for SQS calculations, we first calculate $\Delta H^{(R)}(x = \frac{1}{2})$ using the cluster expansion method of Eqs. (2.9)–(2.13). In Ref. 55, we have used this approach to calculate the mixing enthalpy of the *imperfectly* disordered alloy (i.e., with short-range order).

Major upside of SQS and important fact
to consider for my project.

Since our interest in the present paper is in comparative simulations of the perfectly disordered (random) alloy, we first provide $\Delta H(x)$ as obtained by cluster expansion in the $T \rightarrow \infty$ (random disorder) limit. By Eqs. (2.7) and (2.8), we see that at $x = \frac{1}{2}$

$$\Delta H^{(R)}\left(\frac{1}{2}\right) = D_{0,1} \varepsilon_{0,1}, \quad (4.2)$$

hence (since $D_{0,1} = 1$), Eq. (2.10) gives

$$\Delta H^{(R)}\left(\frac{1}{2}\right) = \frac{1}{N} \sum_s^{N_s} [\bar{\Pi}_{0,1}(s)]^{-1} E(s), \quad (4.3)$$

where $E(s)$ is the excess energy of the ordered structure s at the equilibrium volume $V(x = \frac{1}{2})$ of the random alloy, and $\bar{\Pi}^{-1}$ is a matrix inverse. Equation (4.3) provides a simple way to calculate the mixing enthalpy of the $x = \frac{1}{2}$ random alloy from the known total energies of N_s periodic structures, without resort to complex solutions of the Ising Hamiltonian. In Ref. 55(a), we illustrated the convergence of Eq. (4.3) for $\text{GaSb}_{0.5}\text{As}_{0.5}$ with respect to the number N_s of periodic structures used in this expansion. We found $\Delta H^{(R)}\left(\frac{1}{2}\right)$ to be (in meV/4 atoms) 140.25, 139.88, 92.63, and 88.69, for $N_s = 3, 5, 6$, and 8 well-selected structures, respectively; other calculations^{55(a)} extending N_s to 10 showed that this result is converged to within ~ 3 meV/4 atoms. We have performed analogous calculations for a series of III-V and II-VI alloys, using the LAPW method for $N_s = 8$ structures described in Ref. 55. The resulting $\Delta H^{(R)}\left(\frac{1}{2}\right)$ values are given in Table VI where they are denoted as “cluster expansion.” An analogous calculation was done for $\text{GaP}_{0.5}\text{As}_{0.5}$ and $\text{Al}_{0.5}\text{Ga}_{0.5}\text{As}$ using the pseudopotential method; the result is also included in Table VI. These $\Delta H^{(R)}$ values will form the benchmark against which calculations on SQS’s can be compared.

2. Using special quasirandom structures

Table VI also gives the mixing enthalpy of Eq. (4.1) calculated directly from the relaxed total energy of the SQS’s for $N=2,4$ and for two systems at $N=8$. We see that a single calculation on SQS-4 or SQS-8 reproduces within a few meV the full cluster expansion result at $x = \frac{1}{2}$ (involving eight structures). While the SQS’s and the cluster expansion method give similar results for the excess energy, only the SQS’s afford direct calculation of real-space quantities (e.g., alloy electronic charge density). Furthermore, the SQS’s avoid direct calculation of ε_f , which also involves truncation of the summation in Eq. (2.10); in this sense, the SQS approach is more accurate than cluster expansion.

It is important to note here the relevance of structural relaxations. Calculations for $\text{GaSb}_{0.5}\text{As}_{0.5}$ with SQS-2 give $\Delta H^{(R)}\left(\frac{1}{2}\right) = 115$ meV/4 atoms for the fully relaxed structure, but $\Delta H^{(R)}\left(\frac{1}{2}\right) = 237$ meV/4 atoms for the unrelaxed structure [experimental estimates, compiled in Ref. 55(b) give 90 ± 10 meV/4 atoms]. For $\text{GaAs}_{0.5}\text{P}_{0.5}$, the relaxed value for SQS-8 is $\Delta H^{(R)}\left(\frac{1}{2}\right) = 16.5$, yet for the unrelaxed structure it is 60.2 meV/4 atoms. The experimental estimate is 18 ± 10 meV/4 atoms. There can be no doubt that structural relaxations, omitted in VCA and SCPA, have an overwhelming effect on the thermodynamics of lattice-mismatched alloys. The effect of sub-lattice relaxation on the *optical* properties will be discussed in Sec. IV E.

Table VI shows a reasonably rapid convergence of the SQS total energy with N . This is particularly true for lattice-matched systems such as $\text{Al}_{0.5}\text{Ga}_{0.5}\text{As}$, for which pseudopotential calculations give $\Delta H^{(R)}\left(\frac{1}{2}\right)$ values of 13.7, 10.5, and 10.5 meV/4 atoms for SQS-2, SQS-4, and SQS-8, respectively. Even for a lattice-mismatched system like $\text{GaP}_{0.5}\text{As}_{0.5}$, the results for $N=2, 4$, and 8 (26.1,

TABLE VI. Mixing enthalpies $\Delta H(x = \frac{1}{2})$ of the random alloy, in meV/4-atoms, as obtained by the LAPW and pseudopotential calculations on SQS’s and from a cluster expansion [Eqs. (2.9)–(2.13)] on eight periodic structures. To achieve convergence in the latter, interactions extending to the fourth fcc neighbors were included.

$\Delta H^{(R)}\left(\frac{1}{2}\right)$	LAPW ^a						Pseudopotential ^b		
	AlAs GaAs	GaSb GaAs	InAs GaAs	GaP InP	HgTe CdTe	ZnTe CdTe	HgTe ZnTe	GaP GaAs	AlAs GaAs
CuPt	7.5	132	108.5	155.4	9.8	103.5	103.3	31.6	10.7
SQS-2	11.5	115	66.7	91.0	12.1	54.2	42.5	26.1	13.7
SQS-4	6.0	80	47.3	73.0	9.8	56.1	49.1	13.9 ^c	10.5 ^d
Cluster expansion ($T = \infty$)	6.6	91	58.8	81.5	8.4	55.3	47.6	19.5	10.5

^a2-k point calculation. For a 10-k-point calculation for GaInP_2 we find for SQS-2 95.0 meV/4 atoms and for GaInAs_2 67.5 meV/4 atoms. For GaAlAs_2 this gives 13.8 for SQS-2 and 9.8 for the CuPt structure. These results are in excellent agreement with the pseudopotential calculations.

^b $E_1 = 15$ Ry and 29 zinc-blende-equivalent k points. With 10 zinc-blende-equivalent k points we get for Ga_2PAs 37.2, and 26.6 meV/4 atoms for CuPt and SQS-2, respectively.

^cFor SQS-8 this gives 16.5 meV/4 atoms.

^dFor SQS-8 this gives 10.5 meV/4 atoms.

13.9, and 16.5 meV/4 atoms, compared with 19.5 in the cluster expansion) appear reasonably well converged.

The fact that $\Delta H^{(R)}$ of random alloys lends itself to calculation in terms of the energy of a *specially oriented* superlattice (Table II) makes it easy to compare the stability of a random alloy with that of *ordinary* superlattices, e.g., the CuPt structure of Table VI. Such a comparison was recently given by Dandrea *et al.*¹⁰³

C. Equilibrium lattice structure

Since the SQS approach affords energy-minimizing relaxation of the alloy structure, it mimics the local alloy geometry. As indicated above, in the VCA to pseudo-binary $A_{1-x}B_xC$ alloys, all $A-C$ and $B-C$ anion-cation bond lengths are assumed equal (to $\sqrt{3}a/4$, where a is the lattice constant at composition x), and all $A-A$, $A-B$, and $B-B$ next-nearest-neighbor distances are taken to be equal (to $a/\sqrt{2}$). In the SCPA approach, $A \neq B$ but $R(A-A)=R(A-B)=R(B-B)$ and there exists only a single type of C site. Figure 2 shows the calculated anion-cation ($A-C$ and $B-C$) bond lengths in $\text{GaP}_{0.5}\text{As}_{0.5}$ as obtained in a pseudopotential calculation for SQS-8; Fig. 3 shows analogous information for the next-nearest-neighbor distances. Both figures indicate distributions of distances, unlike VCA and SCPA where sharp values are assumed for each composition. Regarding the anion-cation bond lengths (Fig. 2), we see that the shorter of the two binary bonds (Ga-P) becomes longer in the alloy while the longer of the two bonds (Ga-As) becomes shorter. These trends are apparent in EXAFS studies.⁴²⁻⁴⁵ To quantify this, we define the bond relaxation function for the $A_xB_{1-x}C$ alloy as

$$\eta(x) = \frac{R_{BC}(x) - R_{AC}(x)}{R_{BC}^0 - R_{AC}^0}, \quad (4.4)$$

where $R_{BC}(x)$ and $R_{AC}(x)$ are the nearest-neighbor bond lengths in an alloy of composition x , and R_{BC}^0 and R_{AC}^0 are the bond lengths in the pure BC and AC zinc-blende

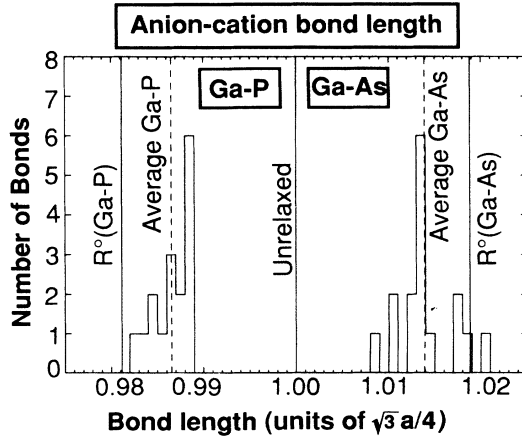


FIG. 2. Distribution of the nearest-neighbor, anion-cation bond lengths in a relaxed SQS-8 model of $\text{GaP}_{0.5}\text{As}_{0.5}$, in units of the unrelaxed ($\sqrt{3}/4a$) bond length. Note that in the alloy, the shorter (Ga-P) bond becomes longer relative to pure GaP, whereas the longer of the two bonds (Ga-As) becomes shorter.

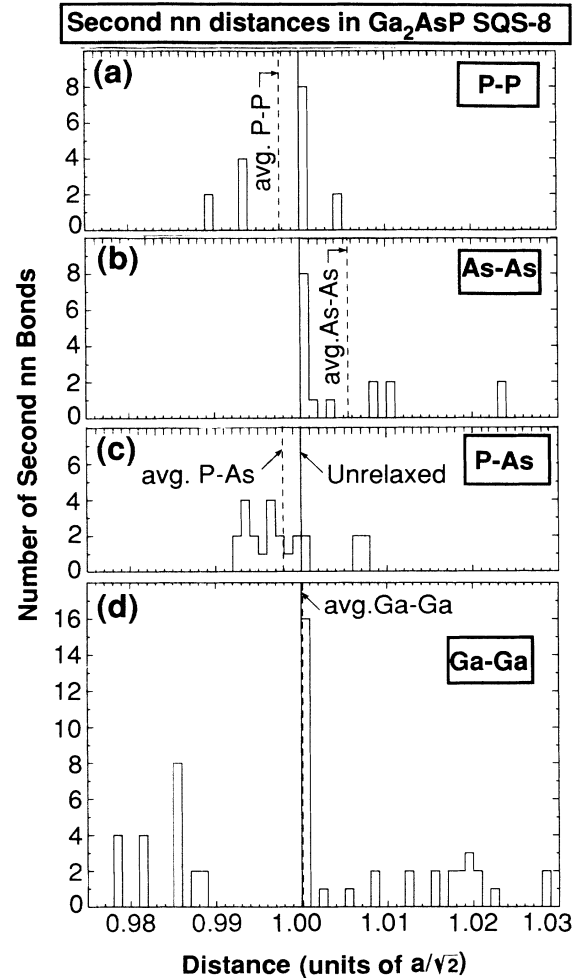


FIG. 3. Distribution of the next-nearest-neighbor distances in the relaxed SQS-8 model of $\text{GaP}_{0.5}\text{As}_{0.5}$, in units of the unrelaxed bond length $a/\sqrt{2}$.

compounds, respectively. In the VCA, $\eta \equiv 0$. If $\eta < 1$, the alloy environment acts to *reduce* the difference between the individual bond lengths relative to the binaries, whereas if $\eta > 1$, the alloy environment *amplifies* the difference. From Fig. 2 we find

$$\eta_{\text{calc}}(x = \frac{1}{2}) = 0.727. \quad (4.5)$$

Boyce and Mikkelsen^{42(b)} measured for $\text{GaAs}_x\text{P}_{1-x}$

$$\begin{aligned} \frac{1}{2}\Delta r_{BC} &= R_{BC}(\frac{1}{2}) - R_{BC}^0 = -0.022/2 \text{ \AA}, \\ -\frac{1}{2}\Delta r_{AC} &= R_{AC}(\frac{1}{2}) - R_{AC}^0 = -0.021/2 \text{ \AA}, \end{aligned} \quad (4.6)$$

and

$$R_{BC}^0 - R_{AC}^0 = 0.088 \text{ \AA}.$$

Hence

$$\eta_{\text{expt}}(\frac{1}{2}) = 1 + \frac{\Delta r_{BC} + \Delta r_{AC}}{2(R_{BC}^0 - R_{AC}^0)} = 0.756, \quad (4.7)$$

in good agreement with our result of Eq. (4.5). A different experimental value of $\eta(\frac{1}{2})=0.55$ was reported by Sasaki *et al.*⁴⁵

The next-nearest-neighbor distances (Fig. 3) exhibit $R(C-C)\neq R(B-B)\neq R(A-A)\neq R(A-B)$. Such relaxation affects both the alloys' formation enthalpies (Sec. II B) and, through the appropriate deformation potentials, the alloy band gaps (Sec. IV F).

D. X-ray structure factors

While the alloy formation enthalpy converges rather rapidly in a cluster expansion (representing largely the effect of the "local" atomic structure), one can surely think of other physical properties that are dominated instead by the long-range order, hence, perhaps not being amenable to a description through SQS's. Such is the diffraction pattern of an alloy, reflecting its long-range periodicity. Using the pseudopotential method we have

calculated self-consistently the Fourier transform of the charge density $\rho(\mathbf{G})$ of $\text{GaP}_{0.5}\text{As}_{0.5}$ in the relaxed SQS-2, SQS-4, and SQS-8 structures, as well as the relaxed chalcopyrite (*CH*), and (*CP*) structures; those x-ray scattering factors are depicted in Fig. 4. In a perfectly random zinc-blende alloy, we expect to find (in addition to the diffuse background) only zinc-blende allowed reflections, denoted in Fig. 4 by solid circles. The additional artificial periodicity of the SQS's generates also zinc-blende "forbidden" reflections evident in Fig. 4. These, however, are rather weak. To measure this, we can define a "quality factor" Q which is the normalized average of all *non-zinc-blende* $\rho(\mathbf{G}_i)$ up to a certain large G_{\max} . In a perfect zinc-blende alloy (and in the VCA), $Q=0$. Figure 4 shows that Q is rather small in SQS-4 ($Q=0.0206$) and SQS-8 ($Q=0.0157$). For comparison, the normalized average over all zinc-blende *allowed* reflections up to the same G_{\max} is 0.9273 in VCA.

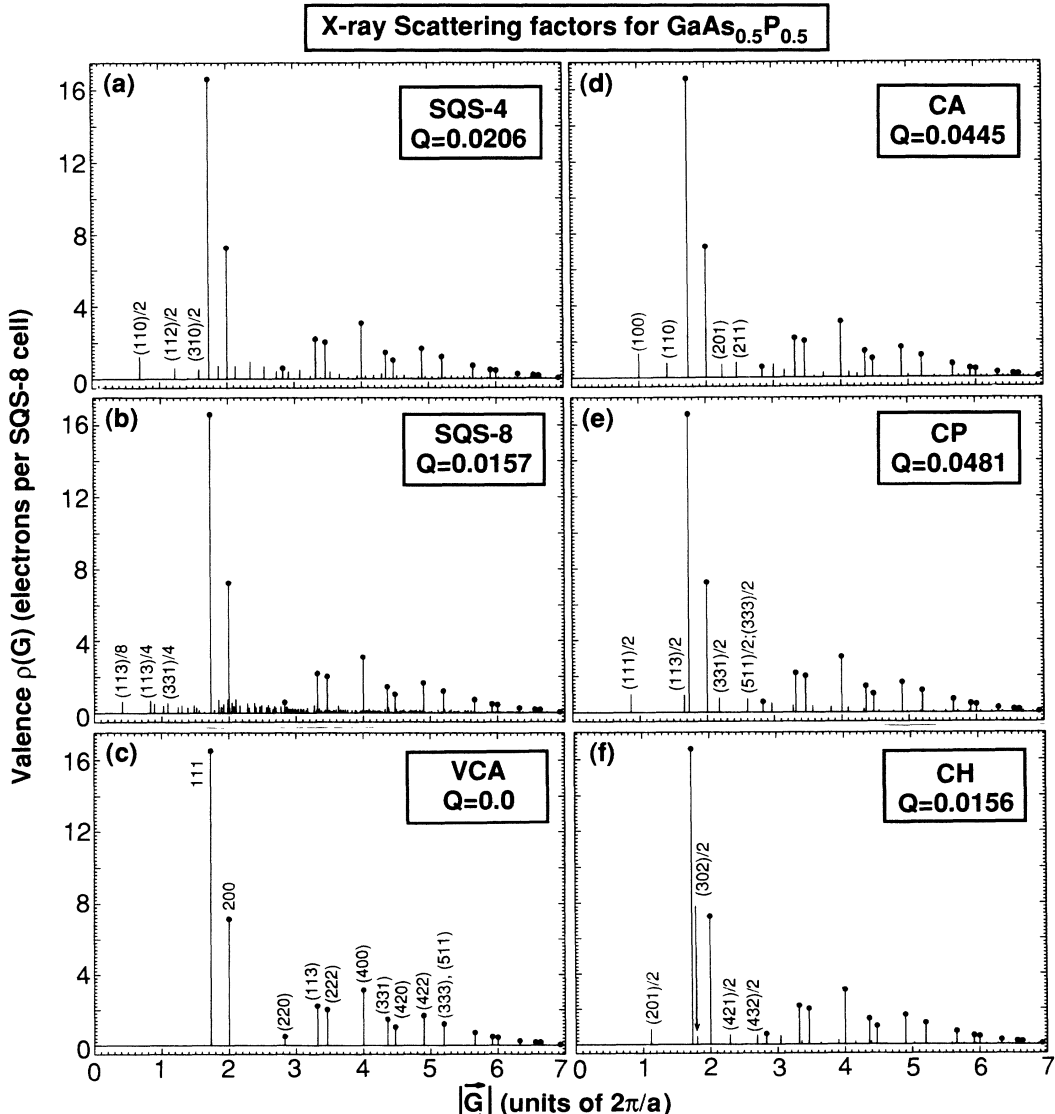


FIG. 4. Self-consistently calculated, pseudopotential x-ray scattering factors of the relaxed SQS models of $\text{GaP}_{0.5}\text{As}_{0.5}$ and of ordered structures at $x=0.5$. The normalization of $\rho(\mathbf{G}=0)$ is $64e/\text{cell}$. Insets give the "quality factor" Q , i.e., the normalized average of zinc-blende *forbidden* reflections; zinc-blende allowed reflections are denoted by solid circles.

E. Electronic structure

The electronic structure of substitutional isovalent semiconductor alloys exhibits a number of experimentally established features.

(i) While band-edge transitions remain nearly as sharp as in the constituents, alloy broadening is observed at other energies.³⁸

(ii) "No-phonon indirect transitions" are observed,^{4,61} while they resemble $\Gamma \rightarrow X$ transitions in the binary, phonons are nevertheless not involved.

(iii) Most transition energies bow downwards with x , i.e., their energies lie below the concentration-weighted average transition energies of the constituents. Different transitions have different bowing parameters.^{1,5}

(iv) Valence-band states observed in photoemission are often split into *A*-like and *B*-like components.⁴⁰

All of the features can be understood qualitatively by noting that SQS's closely approximate the atomic geometry of random alloys and that, at the same time,

these SQS's are *superlattices*. Recall that superlattice states $\Psi_i(\bar{\mathbf{K}}\mathbf{r})$ of band index i and wave vector $\bar{\mathbf{K}}$ can be analyzed in terms of the states $\phi_j(\mathbf{k}, \mathbf{r})$ of the *constituents* using compatibility and "folding" relationships. For example, the (001) superlattice SQS-2 (with repeat period of 1) exhibits the compatibility relations¹⁰⁴ (shown here as appropriate to mixed-cation superlattices with the origin on the anion site)

$$\begin{aligned} \Gamma_{1c}^{\text{ZB}} &\rightarrow \bar{\Gamma}_{1c} , \\ X_{1c}^{\text{ZB}} &\rightarrow \bar{M}_{5c} + \bar{\Gamma}_{4c} , \\ X_{3c}^{\text{ZB}} &\rightarrow \bar{M}_{1c} + \bar{M}_{2c} + \bar{\Gamma}_{1c} , \\ L_{1c}^{\text{ZB}} &\rightarrow \bar{R}_{1c} + \bar{R}_{4c} , \end{aligned} \quad (4.8)$$

where ZB denotes zinc-blende states, and superlattice states are denoted by a bar. Here, $\bar{\Gamma}=(0,0,0)$; $\bar{M}=(0,1,0)$, and $\bar{R}=(\frac{1}{2}, \frac{1}{2}, \frac{1}{2})$ (in Cartesian coordinates with units $2\pi/a$). For SQS-4, we have the folding relations:

$$\begin{aligned} \Gamma^{\text{ZB}}(0,0,0), \quad X_z^{\text{ZB}}(001), \quad \Sigma_{\alpha}^{\text{ZB}}(\frac{1}{2}, \frac{1}{2}, 0), \quad \Sigma_{\alpha}^{\text{ZB}}(-\frac{1}{2}, -\frac{1}{2}, 0) &\rightarrow \bar{\Gamma}(0,0,0) , \\ X_x^{\text{ZB}}(100), \quad X_y^{\text{ZB}}(010), \quad \Sigma_{\beta}^{\text{ZB}}(\frac{1}{2}, -\frac{1}{2}, 0), \quad \Sigma_{\beta}^{\text{ZB}}(-\frac{1}{2}, \frac{1}{2}, 0) &\rightarrow \bar{X}(-\frac{1}{2}, \frac{1}{2}, 0) , \\ L_1^{\text{ZB}}(\frac{1}{2}, \frac{1}{2}, \frac{1}{2}), \quad L_2^{\text{ZB}}(\frac{1}{2}, \frac{1}{2}, -\frac{1}{2}), \quad \Delta_{\alpha}^{\text{ZB}}(0, 0, \frac{1}{2}), \quad \Delta_{\alpha}^{\text{ZB}}(0, 0, -\frac{1}{2}) &\rightarrow \bar{Y}(0, 0, \frac{1}{2}) , \\ L_3^{\text{ZB}}(-\frac{1}{2}, \frac{1}{2}, \frac{1}{2}), \quad L_4^{\text{ZB}}(\frac{1}{2}, -\frac{1}{2}, \frac{1}{2}), \quad W_{\alpha}^{\text{ZB}}(0, 1, \frac{1}{2}), \quad W_{\alpha}^{\text{ZB}}(1, 0, \frac{1}{2}) &\rightarrow \bar{S}(\frac{1}{2}, -\frac{1}{2}, \frac{1}{2}) . \end{aligned} \quad (4.9)$$

In general, we can expand a given zinc-blende state in a complete set of superlattice states; i.e.,

$$\phi_j^{\text{ZB}}(\mathbf{k}, \mathbf{r}) = \sum_{\mathbf{K}} \sum_i^{\text{SQS}} A_{ij}(\bar{\mathbf{K}}, \mathbf{k}) \psi_i^{\text{SQS}}(\bar{\mathbf{K}}, \mathbf{r}) . \quad (4.10)$$

The inverse expansion is also possible; i.e.,

$$\psi_i^{\text{SQS}}(\bar{\mathbf{K}}, \mathbf{r}) = \sum_{\mathbf{k}} \sum_j^{\text{ZB}} B_{ij}(\bar{\mathbf{K}}, \mathbf{k}) \phi_j^{\text{ZB}}(\mathbf{k}, \mathbf{r}) . \quad (4.11)$$

Table VII illustrates Eq. (4.10) for GaAs_{0.5}P_{0.5} in SQS-8. For each of the principal zinc-blende states we show the states in the SQS's that have the highest weights $|A_{ij}(\bar{\mathbf{K}}, \mathbf{k})|^2$. Table VIII illustrates the expansion (4.11).

Using the terminology of superlattice theory, we next discuss the salient features of the electronic structure of the random alloy as modeled by SQS's.

(i) *Crystal-field splitting*. States that are degenerate in the ZB structure [e.g., the Γ_{15v} valence-band maximum (VBM)] can be split in the SQS or in other ordered structures by the reduced symmetry of the crystal field (see Γ_{15v} in Table II). In the ordered structures *CA*, *CP*, and *CH*, the crystal field splits the triply degenerate Γ_{15} VBM state into a singly and a doubly degenerate state. We define Δ_{CF} to be negative if the singly degenerate state is above the doubly degenerate state. (This is the case in some *CH* compounds and in most of the SQS-4 and SQS-8 structures.) For SQS-4 and SQS-8, the doubly degenerate state is further split by a small amount into two nondegenerate states because of the yet lower symmetry.

In addition, all VBM states are split by the spin-orbit interaction Δ_0 . The two splittings Δ_{CF} and Δ_0 are coupled. The energies of the three components can be described well by Hopfield's quasicubic model;¹⁰⁵ relative to their center of gravity, they are

$$E_{1,2,3} = \begin{cases} \frac{1}{3}(\Delta_0 + \Delta_{\text{CF}}) , \\ -\frac{1}{6}(\Delta_0 + \Delta_{\text{CF}}) \pm \frac{1}{2}[(\Delta_0 + \Delta_{\text{CF}})^2 - \frac{8}{3}\Delta_0\Delta_{\text{CF}}]^{1/2} . \end{cases} \quad (4.12)$$

We have fitted our calculated relativistic VBM energy levels to Eq. (4.12) and extracted Δ_0 and Δ_{CF} given in Table IX. We see that the crystal-field splitting of the VBM is relatively small in the SQS structures and is likely to be even smaller in actual random alloy samples because of the existence of differently oriented nonrandom domains. However, it can be sizable in ordered alloys where all domains are coherently aligned. The Δ_0 and Δ_{CF} splittings are analogous to the heavy-hole versus light-hole splitting in superlattices.

(ii) *Pseudodirect transitions*. Because of zone folding, states in the SQS structures at the center $\bar{\Gamma}$ of the Brillouin zone can evolve from either Γ^{ZB} states [e.g., $\bar{\Gamma}(\Gamma_{1c})$, a state connected to the VBM by truly direct transitions], or from non- Γ^{ZB} states [e.g., $\bar{\Gamma}(L_{1v}^{\text{ZB}})$ and $\bar{\Gamma}(L_{1c}^{\text{ZB}})$ of Table VI]. This is illustrated in Table VII under the fifth column (headed " $\bar{\Gamma}$ "). This introduces the possibility of "pseudodirect" transitions, for example, between $\bar{\Gamma}(\Gamma_{15v}^{\text{ZB}})$

TABLE VII. Pseudopotential energy levels ($E_1 = 15$ Ry, 29 zinc-blende-equivalent \mathbf{k} points) of the relaxed SQS-8 for $\text{GaAs}_{0.5}\text{P}_{0.5}$ at high-symmetry points. States with more than 20% zinc-blende Γ , X , or L character are shown. For each zinc-blende state we give the SQS state folded from it [Eq. (4.10)]. Averages of the zinc-blende energy levels (over GaP and GaAs) are given both at the binary equilibrium lattice constants (a_{eq}) and at the alloy lattice constant (\bar{a}). All values are in eV. NF indicates that the corresponding zinc-blende state is “nonfolding” into this sublattice state.

ZB state	Average of binaries	Average of binaries	VCA	$\bar{\Gamma} = (0,0,0)$	GaAs _{0.5} P _{0.5} SQS-8 states		
	(a_{eq})	(\bar{a})			$\bar{\mathbf{K}} = \frac{2\pi}{a}(\frac{1}{4}, \frac{1}{4}, -\frac{1}{4})$	$\bar{\mathbf{K}} = \frac{2\pi}{a}(\frac{3}{8}, -\frac{5}{8}, \frac{1}{8})$	
					\bar{A}	$\bar{\theta}$	
Γ_{1v}	-12.66	-12.67	-12.74	-12.74	NF		NF
L_{1v}	-10.79	-10.78	-10.85	-10.92	-10.78		-11.04 ^a ; -10.87 ^a
X_{1v}	-9.93	-9.95	-10.02	NF	-9.96		-9.89
X_{3v}	-6.87	-6.87	-6.90	NF	-6.92		-6.94
L_{1v}	-6.73	-6.73	-6.76	-6.80	-6.78		-6.80
X_{5v}	-2.72	-2.73	-2.74	NF	-2.83; -2.80		-2.83; -2.82; -2.76; -2.66
L_{3v}	-1.15	-1.14	-1.15	-1.18 ^a ; -1.18; -0.96 ^a	-1.28; -1.18		-1.19; -1.15
Γ_{15v}	0.0	0.0	0.0	-0.061; -0.049; 0.0	NF		NF
X_{1c}	1.45	1.45	1.43	NF	1.38		1.35; 1.38 ^b
L_{1c}	1.41	1.42	1.40	1.35	1.35		1.35 ^b ; 1.38 ^b
X_{3c}	1.67	1.67	1.67	NF	1.53		-1.61
Γ_{1c}	1.44	1.41	1.37	1.36	NF		NF
Γ_{15c}	3.83	3.84	3.84	3.77; 3.80; 3.84	NF		NF
L_{3c}	4.67	4.69	4.69	4.60; 4.63	4.49 ^a ; 4.54; 4.83 ^a		4.52 ^a ; 4.58 ^a ; 4.93 ^a

^aThese states are of mixed character.

^b $X_{1c} + L_{1c}$.

TABLE VIII. Square of the expansion coefficients of some SQS-8 pseudopotential wave function in terms of a set of zinc-blende VCA wave functions [Eq. (4.11)]. The point denoted \bar{A} is $(2\pi/a)(\frac{1}{4}, \frac{1}{4}, -\frac{1}{4})$, and $\bar{\theta}$ is $(2\pi/a)(\frac{3}{8}, -\frac{5}{8}, \frac{1}{8})$.

Label	SQS states	Energy	Spectral weight $ B_{ij}(\mathbf{k}, \mathbf{r}) ^2$				
			From Γ_{1v}^{ZB}	From L_{1v}^{ZB}	From $X_{\beta v}^{\text{ZB}}$ ^a	From L_{1c}^{ZB}	From $X_{\beta c}^{\text{ZB}}$ ^a
$\text{GaAs}_{0.5}\text{P}_{0.5}$							
$\bar{\Gamma}(\Gamma_{1v})$	-12.74	0.98	0	0	0	0	0
$\bar{\Gamma}_{1v}$	-10.92	0	0.80	0	0	0	0
$\bar{\Gamma}(L_{1c})$	1.35	0	0	0	0.98	0	0
$\bar{\Gamma}(\Gamma_{1c})$	1.36	0	0	0	0	0	0.99
$\bar{\theta}(L_{1c} + X_{1c})$	1.35	0	0	0	0.74	0.23	0
$\bar{\theta}(X_{1c} + L_{1c})$	1.38	0	0	0	0.25	0.74	0
$\text{Al}_{0.5}\text{Ga}_{0.5}\text{As}$							
$\bar{\Gamma}(\Gamma_{1v})$	-12.43	0.97	0	0	0	0	0
$\bar{A}(X_{3v} + L_{1v})$	-6.28	0	0.31	0.63	0	0	0
$\bar{A}(L_{1v} + X_{3v})$	-6.24	0	0.66	0.32	0	0	0
$\bar{\Gamma}(\Gamma_{1c})$	1.38	0	0	0	0	0	0.91
$\bar{A}(L_{1c})^b$	1.38	0	0	0	0.68	0.03	0
$\bar{\Gamma}(L_{1c})$	1.49	0	0	0	0.92	0	0
$\bar{A}(X_{3c} + L_{1c})$	1.74	0	0	0	0.11	0.71	0
$\bar{A}(X_{3c} + L_{1c})$	2.34	0	0	0	0.12	0.18	0

^a $\beta = 1$ for $\text{GaAs}_{0.5}\text{P}_{0.5}$; $\beta = 3$ for $\text{Al}_{0.5}\text{Ga}_{0.5}\text{As}$.

^bThis state also has $\sim 0.07 X_{1c}$ character.

TABLE IX. LAPW calculated crystal-field splitting Δ_{CF} and spin-orbit splitting Δ_0 (all in eV) at the VBM [from Eq. (4.12)] for seven disordered 50%-50% semiconductor alloys and some of their ordered structures. For comparison, we also give the calculated binary-averaged values. The LDA correction (<0.03 eV for III-V and <0.10 eV for II-VI) for Δ_0 is not included in the binary-averaged value.

System	Property	Binary average	CA	CH	CP	SQS-4
GaInP ₂	Δ_{CF}	0	0.191	0.032	0.212	-0.092
	Δ_0	0.107	0.114	0.108	0.118	0.110
GaInAs ₂	Δ_{CF}	0	0.134	0.020	0.121	-0.064
	Δ_0	0.351	0.355	0.352	0.347	0.347
Ga ₂ AsSb	Δ_{CF}	0	0.085	-0.013	0.230	-0.207
	Δ_0	0.523	0.554	0.522	0.595	0.539
AlGaAs ₂	Δ_{CF}	0	0.049	-0.007	0.028	-0.010
	Δ_0	0.319	0.317	0.319	0.320	0.320
ZnCdTe ₂	Δ_{CF}	0	0.127	0.020	0.099	-0.037
	Δ_0	0.873	0.864	0.868	0.854	0.846
ZnHgTe ₂	Δ_{CF}	0	0.231	0.002	0.257	-0.086
	Δ_0	0.831	0.831	0.828	0.793	0.798
CdHgTe ₂	Δ_{CF}	0	0.008	-0.004	0.020	-0.012
	Δ_0	0.817	0.813	0.812	0.811	0.804

and $\bar{\Gamma}(L_{1c}^{\text{ZB}})$ in SQS-8, that involve no phonons and are temperature independent.^{4,61} However, these folded states largely retain the character of the corresponding unfolded ZB wave functions (e.g., L), and the calculated dipole oscillator strengths for the pseudodirect transitions are generally far smaller than those for the truly direct transitions. Pseudodirect transitions have also been found in SCPA calculations³⁰ but are absent in the VCA.³⁰

(iii) *Interband mixing.* In some cases, individual ZB states can have nonzero projections $A_{ij}(\bar{\mathbf{k}}, \mathbf{k})$ [Eq. (4.10)] onto more than one SQS state, even at the same SQS $\bar{\mathbf{k}}$ point (i.e., not a zone-folding effect). This is the case in $\bar{\theta}(X_{1c})$ and $\bar{\theta}(L_{1v})$ in Table VII. Conversely, individual SQS states can have nonzero projections $B_{ij}(\bar{\mathbf{k}}, \mathbf{k})$ [Eq. (4.11)] onto more than one ZB state. This is the case in $\bar{\theta}(L_{1c} + X_{1c})$ of Table III. Some of the states listed in Table VII show such interband mixing effects, resulting in some cases in the listing of more SQS-8 energy levels than the number (including degeneracy) of ZB Γ , X or L states to which they correspond. [However, if one adds the coefficients $|B_{ij}(\bar{\mathbf{k}}, \mathbf{k})|^2$ for a set of SQS states corresponding to a particular ZB level, the correct number of states (i.e., the degeneracy of the ZB level) is obtained.] Table VIII shows $|B_{ij}(\bar{\mathbf{k}}, \mathbf{k})|^2$ for some selected states of GaAs_{0.5}P_{0.5} and Al_{0.5}Ga_{0.5}As in the SQS-8 structure (the sum rule is not necessarily satisfied by the subset of states shown in this table). This illustrates the existence of SQS states of nearly pure single-state ZB character, such as $\bar{\Gamma}(\Gamma_{1v})$, $\bar{\Gamma}(\Gamma_{1c})$, and $\bar{\Gamma}(L_{1c})$, as well as the existence of mixed states such as $\bar{\theta}(X_{1c} + L_{1c})$ and $\bar{\theta}(L_{1c} + X_{1c})$ in GaAs_{0.5}P_{0.5} SQS-8, and $\bar{M}(X_{3c} + L_{1c})$ and $\bar{M}(L_{1c} + X_{3c})$ in Al_{0.5}Ga_{0.5}As SQS-8. This interband mixing represents the effect of the piece of the SQS potential that lacks ZB symmetry. It exists also in SCPA calculations; however, there the mixing potential represents only the *chemical* perturbation due to $A \neq B$, not the *structural* piece due to

relaxation. Figure 5 shows the square of the wavefunction amplitude for some pure [(a) and (b)] and mixed [(c) and (d)] conduction bands in GaAs_{0.5}P_{0.5} SQS-8. Note that, whereas in the SCPA approach all atoms of a given chemical type are assumed to be equivalent, Fig. 5 shows clearly different amplitudes on different atoms of the same chemical type.

Although symmetry permits mixing of the *s*-like Γ_{1c}^{ZB} with the *p*-like Γ_{15v}^{ZB} into the VBM of the SQS's, we find this interband mixing to be exceedingly small ($|B|^2 \approx 0.0005$ in GaAs_{0.5}P_{0.5} SQS-8, and even less in Al_{0.5}Ga_{0.5}As SQS-8). This disproves the hypothesis¹⁰⁶ that the bowing of the spin-orbit splitting reflects interband *s-p* mixing.

(iv) *Alloy broadening.* Individual ZB levels can transform in the SQS structures into a number of levels through the mechanisms of crystal-field splitting, zone folding (of equivalent ZB \mathbf{k} points into inequivalent SQS $\bar{\mathbf{k}}$ points), and interband mixing, all of which were illustrated earlier. As a consequence, transitions characteristic of the ZB structure (e.g., E_0 , E_1 , and E_2) will generally be expected to broaden into several transitions of different energy in the SQS structures. However, the ZB Γ point only maps into a single SQS $\bar{\mathbf{k}}$ point ($\bar{\Gamma}$), and we observe exceedingly small interband mixing of states originating from Γ^{ZB} states. Hence the small broadening of the E_0 transition reflects only the relatively small crystal-field splitting of the VBM. In contrast, the zinc blende L and X states can be split by all three effects, resulting in substantial broadening of the E_1 and E_2 transitions. This is shown in Figs. 6 and 7 for GaAs_{0.6}P_{0.5} in the SQS-8 structure, along with the oscillator strengths for these transitions in the VCA alloy. The analogy between random alloys and SQS's hence clarifies alloy broadening effects in terms of three distinct contributions: crystal-field splitting, zone folding, and interband mixing. In size-mismatched alloys, all three are strongly

affected by structural relaxations.

(v) *Sublattice localization*. In the VCA, there are no distinct spectral signatures of the individual *A* and *B* atoms in $A_{1-x}B_x$; consequently, all states are delocalized. Figure 8 shows the calculated density of states (DOS) of $Cd_{0.5}Hg_{0.5}Te$ in the SQS-4 structure, where distinct peaks associated with Hg *s* and Cd *s* states appear both at the bottom of the upper valence band and near the top of the first conduction band; these can be identified by comparing the angular-momentum-decomposed local DOS [Figs. 8(a)–8(d)]. This non-VCA behavior reflects the disparity between the atomic *s* potentials of these cations, and has been observed in photo-

emission spectra^{40(a)} and explained in CPA calculations.^{40(a)} Likewise, the cation *d* states appear at distinctly different energies. Figure 9 shows a similar splitting in the cation *s* states in $Al_{0.5}Ga_{0.5}As$; Refs. 40(b) and 40(c) discuss this effect. In the SCPA, there is only a single sublattice for each chemical type. Figures 8(a), 8(b), 9(a), and 9(b) show that the two inequivalent anion sites in SQS-4 $Cd_{0.5}Hg_{0.5}Te$ and $Al_{0.5}Ga_{0.5}As$ have slightly different *p*-electron states at the bottom of the upper valence band. Differences in the charge states of the common *C* atoms in the alloy have indeed been observed.^{57,58} Note that the local DOS depends on the size of the muffin-tin (MT) sphere.⁸² (We used $R_{MT} = 1.403 \text{ \AA}$

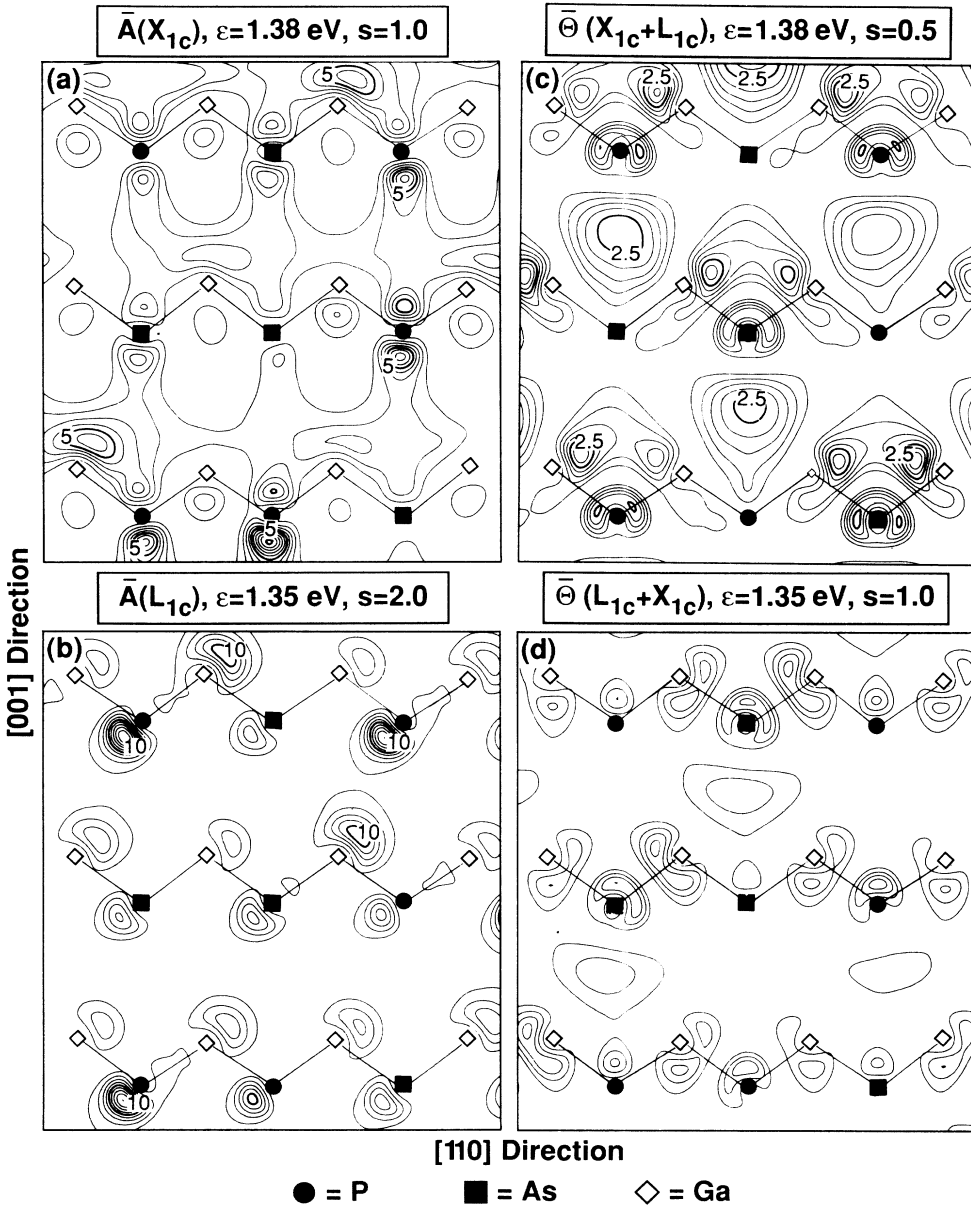


FIG. 5. Pseudopotential calculation of the square of the wave function amplitude for zinc-blende *X*- and *L*-folded conduction states at the \bar{A} (a), (b) and $\bar{\Theta}$ (c), (d) points of Ge_2AsP in the SQS-8 structure. (a) and (b) are nearly pure zinc-blende-like states, whereas (c) and (d) are mixed states, having both *X* and *L* character (in this case, the dominant character is listed first). ϵ denotes the energy level relative to VBM and s denotes the contour step in units of e/cell .

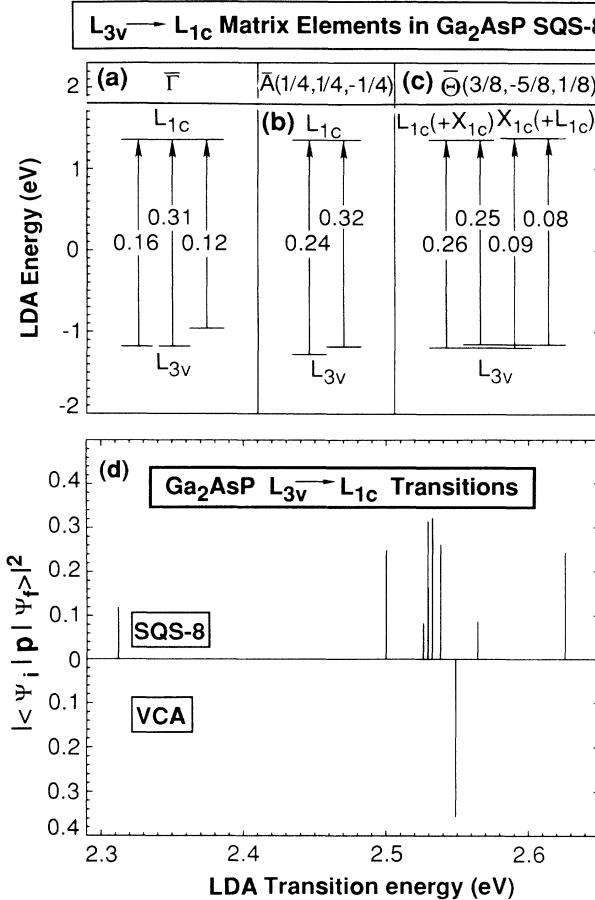


FIG. 6. The square of the dipole matrix element $|\langle \psi_i | \mathbf{p} | \psi_f \rangle|^2$ is shown for transitions between states with more than 20% zinc blende L_{3v} or L_{1c} character [Eq. (4.11)] in Ga_2AsP in the SQS-8 structure. The transition energies have not been corrected for the LDA band-gap error. Reciprocal lattice vectors are in units of $2\pi/a$. (a) Superlattice $\bar{\Gamma}=(0,0,0)$ states, (b) superlattice $\bar{A}=(\frac{1}{4}, \frac{1}{4}, \frac{1}{4})$, and (c) superlattice $\bar{\theta}=(\frac{3}{8}, -\frac{5}{8}, \frac{1}{8})$ states. (d) Spectral representation of (a)–(c), compared with VCA.

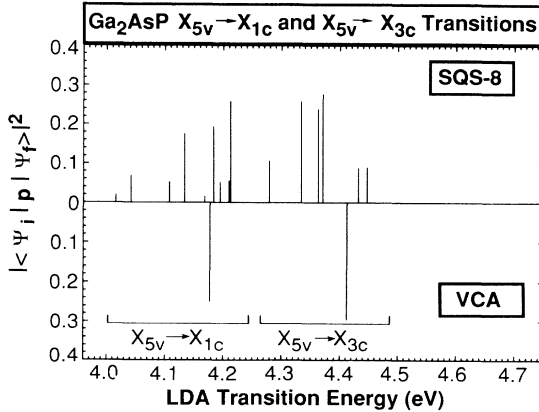


FIG. 7. Square of the dipole matrix element $|\langle \psi_i | \mathbf{p} | \psi_f \rangle|^2$ vs transition energy for transitions between states having more than 20% zinc blende X_{5v} , X_{1c} , or X_{3c} character [Eq. (4.7)] in Ga_2AsP in the SQS-8 structure. The transition energies have not been corrected for the LDA band-gap error.

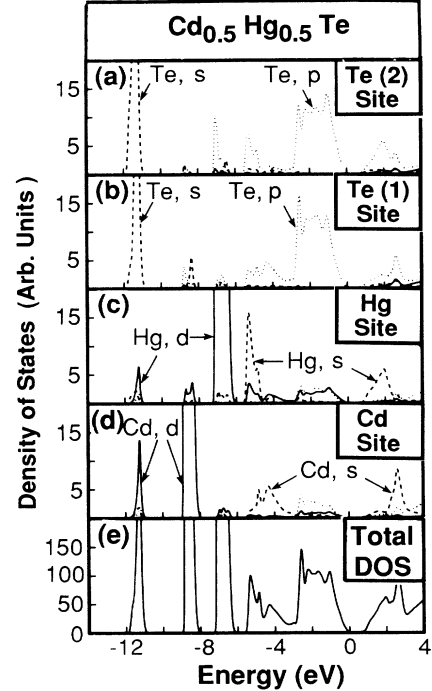


FIG. 8. LAPW-calculated semirelativistic angular momentum and site-projected local density of states (DOS) (a)–(d) and the total DOS (e) for $\text{Cd}_{0.5}\text{Hg}_{0.5}\text{Te}$ in the SQS-4 structure. The dashed lines, dotted lines, and solid lines in (a)–(d) represent s , p , and d states, respectively.

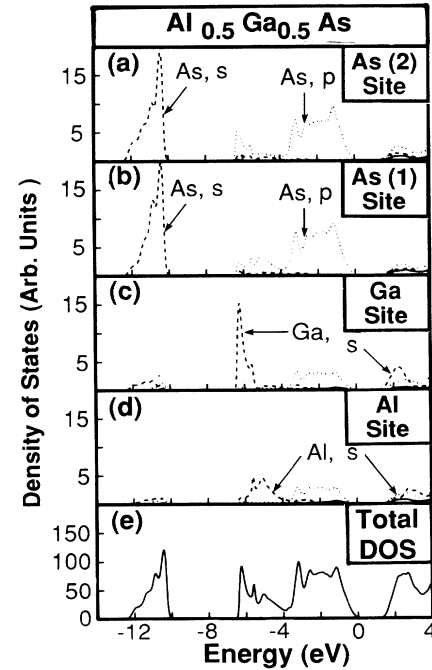


FIG. 9. LAPW-calculated semirelativistic angular momentum and site-projected local density of states (DOS) (a)–(d) and the total DOS (e) for $\text{Al}_{0.5}\text{Ga}_{0.5}\text{As}$ in the SQS-4 structure. The dashed lines, dotted lines, and solid lines in (a)–(d) represent s , p , and d states, respectively.

for atoms of CdHgTe and $R_{MT} = 1.199 \text{ \AA}$ for atoms of $\text{Al}_{1-x}\text{Ga}_x\text{As}$.

Examples of wave functions at $\bar{\Gamma}$ in $\text{GaAs}_{0.5}\text{P}_{0.5}$ in the SQS-8 structure are shown in Figs. 10 and 11. In Fig. 10, only states arising from Γ^{ZB} states are shown, and they are contrasted with the corresponding VCA states. Here there is a similarity between the SQS-8 and VCA states, except for a noticeable difference in the amplitudes on the As and P atoms in the Γ_{1v} state [Figs. 10(c) and 10(d)]. In Fig. 11, states arising from L^{ZB} states are shown. In this case, there are relatively large variations in the amplitude on different types of atoms (unlike VCA), and [especially in Fig. 11(d)] even large variations in the amplitude on chemically identical atoms lying at inequivalent sites (unlike CPA).

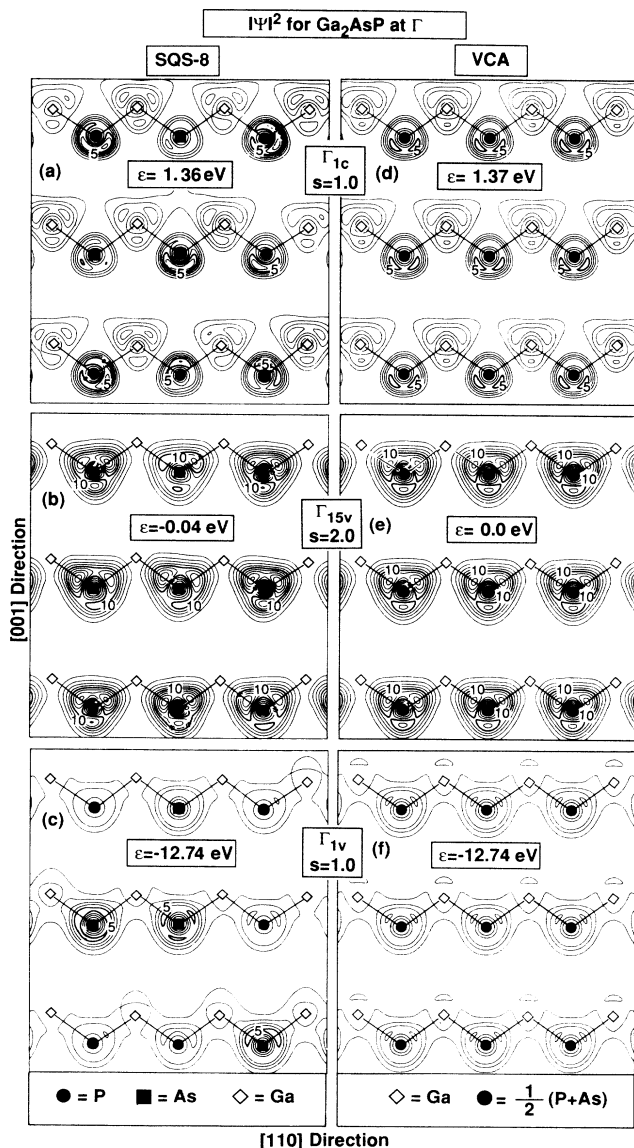


FIG. 10. Pseudopotential calculation of the square of the wave-function amplitude for zinc-blende, Γ -derived states of Ga_2AsP in the SQS-8 structure (a)–(c), and the corresponding VCA states (d)–(f). ϵ denotes the crystal-field averaged eigenvalue and s denotes the contour step in units of e/cell .

F. Optical bowing and its origins

Equations (4.8) and (4.9) and Table VII show how distinct zinc-blende states give rise to a set of closely spaced SQS states of compatible symmetry. Since the experimental definition of optical bowing is based on identifying alloy transitions that evolve from the corresponding transitions in the zinc-blende constituents, we will follow this procedure. For SQS-4, for example, the states corresponding to the high-symmetry ZB states are

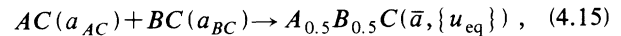
$$\begin{aligned}\Gamma^{\text{ZB}} &= \bar{\Gamma}, \\ L^{\text{ZB}} &= \frac{1}{4}(2\bar{Y} + 2\bar{S}), \\ X^{\text{ZB}} &= \frac{1}{3}(\bar{\Gamma} + 2\bar{X}),\end{aligned}\quad (4.13)$$

where the coefficients on the right-hand side denote degeneracies in the SQS-4 states. The Γ_{15v}^{ZB} valence-band maximum is split in the SQS; the crystal-field average is

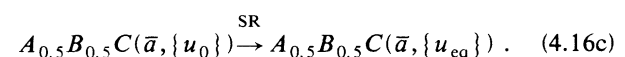
$$\Gamma_{15}^{\text{ZB}} = \frac{1}{3}(\bar{\Gamma}_1 + \bar{\Gamma}_3 + \bar{\Gamma}_4). \quad (4.14)$$

Alloy transition energies from the valence-band maximum Γ_{15}^{ZB} to other final states are hence represented for this purpose by differences between the quantities of Eq. (4.13) and those of Eq. (4.14); this provides the alloy gaps $\epsilon_\lambda(x = \frac{1}{2})$ of Eq. (1.1). Together with the corresponding average transition energies over the binary constituents [first term in square brackets in Eq. (1.1)], this gives the bowing coefficient b_λ at $x = \frac{1}{2}$. Table X summarizes the results obtained this way from calculations on the SQS-4 in a variety of alloys. When available, this table also shows experimental data.¹⁰⁷ We see that SQS-4 represents reasonably well the observed trends (which, unfortunately, show significant scatter). Note that local-density errors are canceled to lowest order since by Eq. (1.1), b_λ represents a difference of eigenvalue differences. Observe in Table X that while b_λ values are positive for most conduction band states, they can be negative for some valence-band states, and that the variation with λ can be substantial for certain alloys.

To analyze the physical origins of bowing, we follow Bernard and Zunger^{37(a)} and decompose b into three components. The overall bowing coefficient at $x = \frac{1}{2}$ measures the change in band gap in the formal reaction



where a_{AC} and a_{BC} are the equilibrium lattice constants of the binary constituents AC and BC , respectively; \bar{a} is the alloy equilibrium lattice constant, and $\{u_{eq}\}$ denotes the equilibrium values of the cell-internal structural parameters of the alloy. We now decompose reaction (4.15) into three steps, namely,



The first step measures the “volume-deformation” (VD) contribution b_{VD} , the second the “charge-exchange” (CE) contribution b_{CE} due to formation of the unrelaxed ($u=u_0$) alloy from $AC+BC$ already prepared at the final lattice constant \bar{a} , and the final step measure changes due to “structural relaxation” (SR), i.e., $u_0 \rightarrow u_{eq}$. The total bowing is

$$b = b_{VD} + b_{CE} + b_{SR}. \quad (4.17)$$

Table XI gives this decomposition for a valence (Γ_{1v}) and conduction (Γ_{1c}) state in the disordered and ordered phases of $\text{GaAs}_{0.5}\text{P}_{0.5}$. It shows that (i) charge-transfer effects can have large contributions to b for valence-band

states of mixed-anion systems but smaller contributions in the conduction band. Note that by Eqs. (4.16), when $a_{AC} \approx a_{BC} \approx \bar{a}$ (lattice-matched alloys), the only contribution is $b=b_{CE}$. (ii) Structural relaxations (neglected in the VCA and the SCPA) are important for both types of states; in this case they reduce b in the valence and can increase it in the conduction band. (iii) The volume-deformation piece (retained in both the VCA and the SCPA) represents as little as one-third of the total valence-band bowing. (iv) The zinc-blende states that fold into the superlattice $\bar{\Gamma}_{1c}$ state depend on the superlattice symmetry: for the common-cation CA structure, X_{1c} and Γ_{1c} fold into $\bar{\Gamma}_{1c}$, while for the chalcopyrite and the CuPt structures, $\Gamma_{1c}+W_{1c}$ and $\Gamma_{1c}+L_{1c}$ fold into

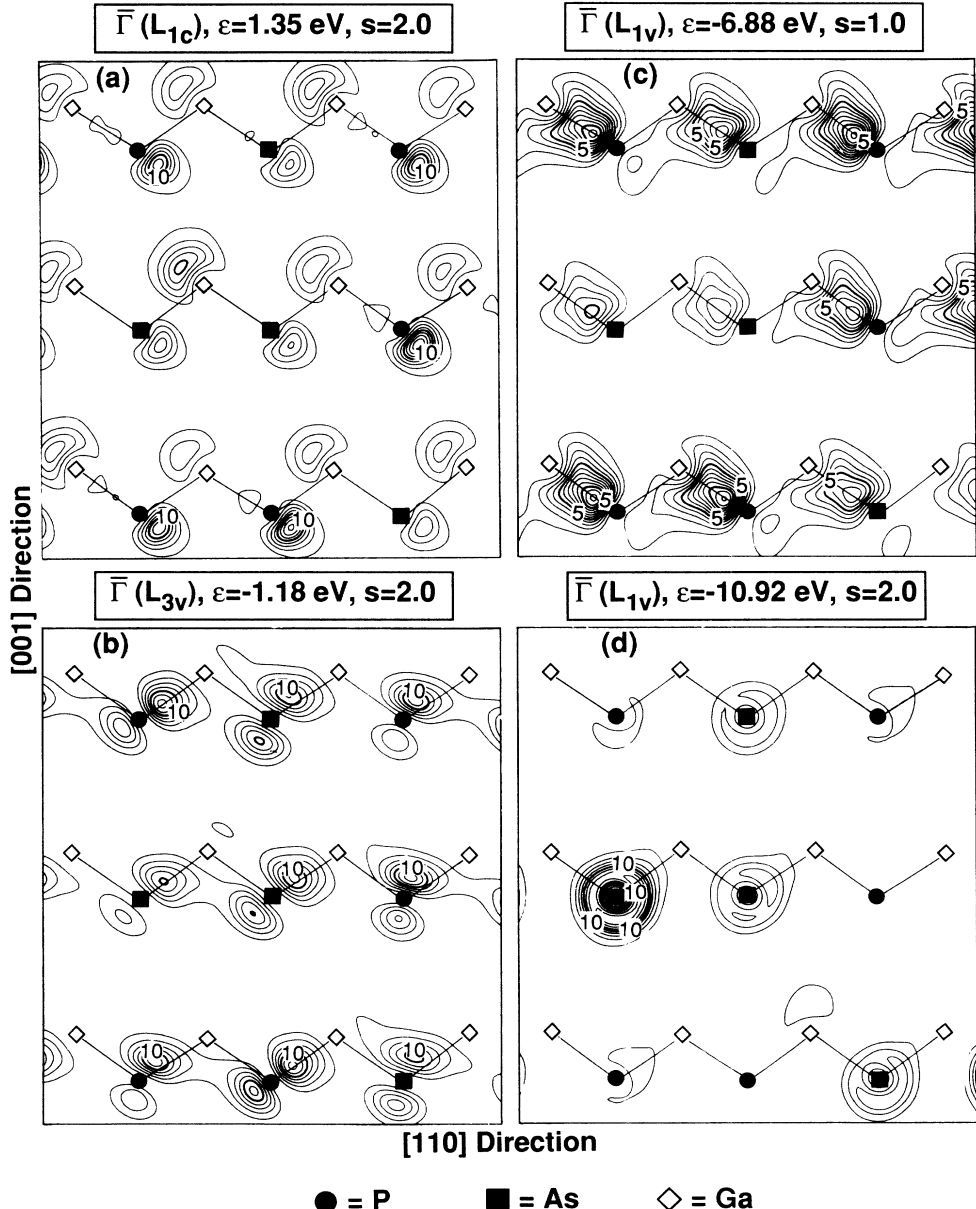


FIG. 11. Pseudopotential calculation of the square of the wave-function amplitude for zinc-blende, L -folded states at the $\bar{\Gamma}$ point of Ga_2AsP in the SQS-8 structure. ϵ denotes the crystal-field averaged eigenvalue and s denotes the contour step in units of e/cell .

TABLE X. LAPW-calculated semirelativistic bowing coefficients (in eV) relative to the VBM, obtained from the relaxed SQS-4 model. We have averaged both over the crystal-field components derived from the VBM states Γ_{1v} and over the final SQS states according to Eqs. (4.13) and (4.14). Full relativistic bowing coefficients can be obtained approximately by subtracting $\frac{1}{3}b(\Delta_0)$ (last row in this table) from the semirelativistic values. The effects are generally small. The last two columns give results of pseudopotential calculations in SQS-4. The results for SQS-8 are very similar (Table XI).

	LAPW						Pseudopotential		
	AlAs GaAs	GaSb GaAs	InAs GaAs	GaP InP	HgTe CdTe	ZNTe CdTe	HgTe ZnTe	AlAs GaAs	GaP GaAs
$b(\Gamma_{1v})$	0.13	0.89	0.03	0.03	0.16	0.02	-0.03	0.06	0.19
$b(\Gamma_{1c})$	0.10	0.61	0.42	0.62	-0.02	0.35	0.23	0.13	0.19
$b_{\text{expt}}(\Gamma_{1c})^a$	0-0.37	1.0-1.2	0.32-0.61	0.65	0-0.23	0.26	0.14	0-0.37	0.17-0.21
$b(\Gamma_{15c})$	0.00	0.12	-0.01	-0.05	-0.04	-0.02	0.01	0.02	0.03
$b(X_{1v})$	0.03	-1.36	-0.02	-0.07	0.04	-0.05	-0.08	-0.01	-0.08
$b(X_{3v})$	0.65	-0.18	0.31	0.14	0.68	0.22	-0.08	0.56	0.08
$b(X_{5v})$	0.00	0.14	-0.05	-0.11	0.04	-0.15	-0.18	0.00	0.05
$b(X_{1c})$	0.01	0.32	0.31	0.31	0.06	0.44	0.45	0.02	0.14
$b(X_{3c})$	0.36	0.51	0.16	0.14	0.80	-0.11	0.87	0.32	0.12
$b(L_{1v})$	-0.03	0.39	-0.07	-0.11	0.00	-0.10	-0.05	-0.05	0.04
$b(L_{1v})$	0.75	0.57	0.63	0.53	0.84	0.24	0.07	0.63	0.14
$b(L_{3v})$	-0.02	-0.23	-0.20	-0.26	-0.01	-0.18	-0.28	-0.03	-0.12
$b(L_{1c})$	0.30	0.39	0.23	0.33	0.26	0.09	0.04	0.30	0.11
$b(\Delta_0)$	0.00	-0.06	0.02	-0.01	0.05	0.11	0.13		

^aReference 107.

$\bar{\Gamma}_{1c}$, respectively. Since these pairs have different energies in the binary constituents, they result in different “level repulsions” in the superlattice, hence different bowing parameters. This is illustrated in Table XI where the crystal-field averaged bowing parameters are given. (v) The bowing coefficients obtained with SQS- N converge rather rapidly with N ; $N=4$ suffices for most purposes.

G. Comparison of band gaps and excess enthalpies of random alloys and ordered structures

Figure 12 compares the calculated bulk formation enthalpy of the random alloy to those of three ordered structures at $x = \frac{1}{2}$: the chalcopyrite (CH), CuAu (CA), and CuPt (CP). As noted previously,^{55,108} the chalcopyrite structure is stabler in bulk form than the random al-

TABLE XI. Decomposition of the optical bowing coefficient (after crystal-field averaging of the VBM) of $\text{GaP}_{0.5}\text{As}_{0.5}$ into “volume deformation” (VD), “charge exchange” (CE), and structural relaxation (SR) pieces; see Eq. (4.16). Results are obtained in an $E_1 = 15$ Ry pseudopotential calculation.

	CH	CP	VCA	SQS-2 CA	SQS-4 Disordered	SQS-8 Disordered
$\Gamma_{1v}-\Gamma_{15v}$						
b_{VD}	0.062	0.062	0.062	0.062	0.062	0.062
b_{CE}	0.251	0.377	0.248	0.249	0.393	0.320 ^a
b_{SR}	-0.181	-0.062	0.000	-0.128	-0.269	-0.200 ^a
b	0.132	0.377	0.310	0.183	0.186	0.183
$\Gamma_{15v}-\Gamma_{1c}$						
b_{VD}	0.125	0.125	0.125	0.125	0.125	0.125
b_{CE}	-0.025	0.056 ^b	0.176	0.125	-0.007	-0.010
b_{SR}	-0.003	-0.077 ^b	0.000	-0.113 ^c	0.068	0.077
b	0.097	0.105	0.302	0.138 ^c	0.186	0.192

^aUsing dipole-oscillator-strength-weighted average of mixed Γ_{1v} states in the unrelaxed geometry.

^bUsing dipole-oscillator-strength-weighted average of strongly mixed Γ_{1c} and L_{1c} states in the unrelaxed geometry.

^cUsing dipole-oscillator-strength-weighted average of strongly mixed Γ_{1c} and X_{1c} states in the relaxed geometry.

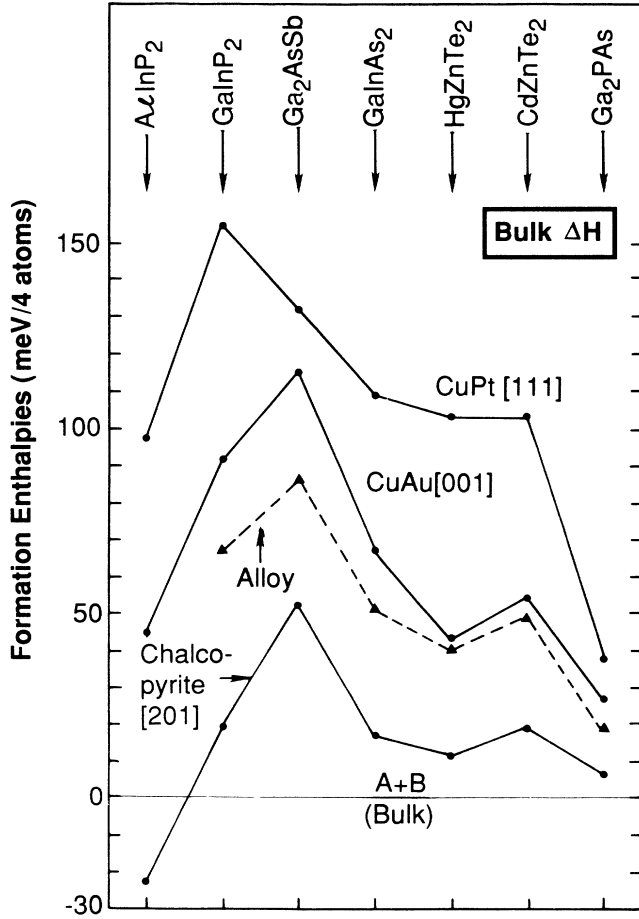


FIG. 12. LAPW-calculated formation enthalpies of seven semiconductor systems in the CuPt, CuAu-I, and chalcopyrite structures, as well as the disordered alloy at $T=800$ K.

loy, hence the latter could metastably order into this structure under bulk growth conditions. On the other hand, both the CuAu and the CuPt structures tend to be of higher energy than the random alloy. However, it has recently been found¹⁰⁹ that *in the presence of a free surface* the stability sequence can be altered relative to the bulk; e.g., the GaInP₂ surface is stabler in the CuPt form than in the chalcopyrite form. If such surface ordering is frozen-in after capping of the surface by the next deposited monolayer, the surface-induced ordering could persist macroscopically. It is likely that this mechanism explains the CuPt ordering observed recently¹¹⁰ in a number of semiconductor alloys.

Since chalcopyrite (Ref. 111), CuAu (Ref. 112), and CuPt (Ref. 110) ordering have been observed in a number of systems, we wish to predict the band gaps in these various structures, and compare them to those of the random alloy. Such calculations within the local-density approximation (LDA) used here face the well-known problem⁸³ of the “band-gap error.” We partially sidestep this problem by (i) calculating within LDA the *change* in the band gap of a given structure relative to equivalent

amounts of the binary constituents [i.e., b_λ of Eq. (1.1)], and then (ii) applying this change to the average of the measured¹⁰⁷ (low-temperature) band gaps of the binary constituents. Since the LDA error largely cancels in step (i), this procedure is likely to produce a reasonable estimate. The results for the predicted direct $\Gamma_{\text{VBM}} \rightarrow \Gamma_{1c}$ gap are given in Fig. 13 where spin-orbit effects have been included. We see that relative to the average gap [$E_g(\text{AC}) + E_g(\text{BC})]/2$, the direct gap decreases in the sequence chalcopyrite \rightarrow random alloy \rightarrow CuAu \rightarrow CuPt. The mechanism for this was discussed in detail by Wei and Zunger⁹⁹ and by Bernard *et al.*¹⁰⁴ These results can be used as a guide for assessing the type of ordering on the basis of the measured direct band gap.

H. Comparison of band gaps of SQS with those obtained by direct sampling

We have recently constructed¹¹³ a periodic model of the $\text{Ga}_{0.5}\text{Al}_{0.5}\text{As}$ alloy by populating randomly a 2304 atom unit cell by Ga and Al (As resides on a separate sublattice). The electronic structure was then described within a tight-binding Hamiltonian whose matrix elements were fit to the band structure of GaAs and AlAs. A spectral weight analysis of the solutions to the 2304 atom cell produced the alloy band gaps (given in eV, with respect to the valence-band maximum):

$$\begin{aligned} & 2.215(\Gamma_{1c}), \quad 2.185(L_{1c}), \quad 2.145(X_{1c}), \\ & 2.645(X_{3c}) \quad (2304 \text{ atoms}). \end{aligned} \quad (4.18)$$

Using SQS-8 with the same tight-binding Hamiltonian yielded the band gaps

$$\begin{aligned} & 2.217(\Gamma_{1c}), \quad 2.196(L_{1c}), \quad 2.160(X_{1c}), \\ & 2.640(X_{3c}) \quad (16 \text{ atoms}), \end{aligned} \quad (4.19)$$

i.e., within ~ 0.02 eV of the 2304-atom/cell calculation. Since structural relaxation is absent in this system, SCPA calculations¹¹³ also give similar results. Notice that the band gap of AlGaAs₂ strongly depends on its crystal structure (Table XII below), hence the success of SQS is significant. Comparing the *width* of the spectral functions for particular states (as measured by the second moment) shows excellent agreement between SQS, the large supercell approach, and SCPA: the CPA “lifetime” broadening is hence captured accurately by the SQS’s. Hence the SQS describes correctly spectral functions of *individual* states, not just averaged quantities. This example illustrates the fact that the SQS is useful in describing optical properties despite the imposition of periodic boundary conditions (since the width reflects primarily the existence of a distribution of *local* environments, described by the SQS).

V. CLUSTER EXPANSION OF THE BAND-GAP ENERGIES

The cluster expansion of Eq. (2.9) has been shown by Sanchez, Ducastelle, and Gratias⁷⁴ to hold for *any* property that can be defined on a fixed lattice, hence, it can also be applied to band gaps. One needs, however, to ex-

amine the rate of convergence. This is done as follows: Using band theory we have first calculated the direct $\Gamma_{15v} \rightarrow \Gamma_{1c}$ band gap $E_g(s)$ of N_s ordered structures $s = AC, BC, CuAu\text{-like}(CA), chalcopyrite(CH), CuPt\text{-like}(CP)$, the $(AC)_2(BC)_2(001)$ superlattice (denoted Z2) and SQS-4. These values, evaluated at the average alloy lattice constant $\bar{a} = (a_{AC} + a_{BC})/2$ and averaged over crystal-field splitting are given in the first eight columns of Table XII. Using Eq. (2.10), we then find the N_s “band-gap interaction energies” ε_f for each alloy. These are then used [Eq. (2.9)] to predict the band gap of SQS-8, and that of the perfectly random alloy [using Eq. (4.3)]. To the extent that the cluster expansion is converged, the two results should be similar. Comparison is given in

Table XII for $N_s = 5, 6$, and 7. We find the following: (i) The cluster expansion works well for Γ_{1c} states of semiconductors, as evidenced by the good agreement between the predicted $E_g(\text{SQS-8})$ values, obtained from the cluster expansion, and the directly calculated value obtained by applying the pseudopotential method to SQS-8 (Table XIII). For $\text{GaAs}_{0.5}\text{P}_{0.5}$ we have calculated, using the pseudopotential method, $E_g(\text{SQS-}N)$ for three SQS’s, finding 1.51, 1.40, and 1.40 eV for $N = 2, 4$, and 8, respectively (Table XIII), demonstrating that SQS-4 is already adequate to find a stable value for the band gap.

(ii) Using 5-, 6-, or 7-ordered structures in the cluster expansion of Eq. (2.9) produces rather similar values for

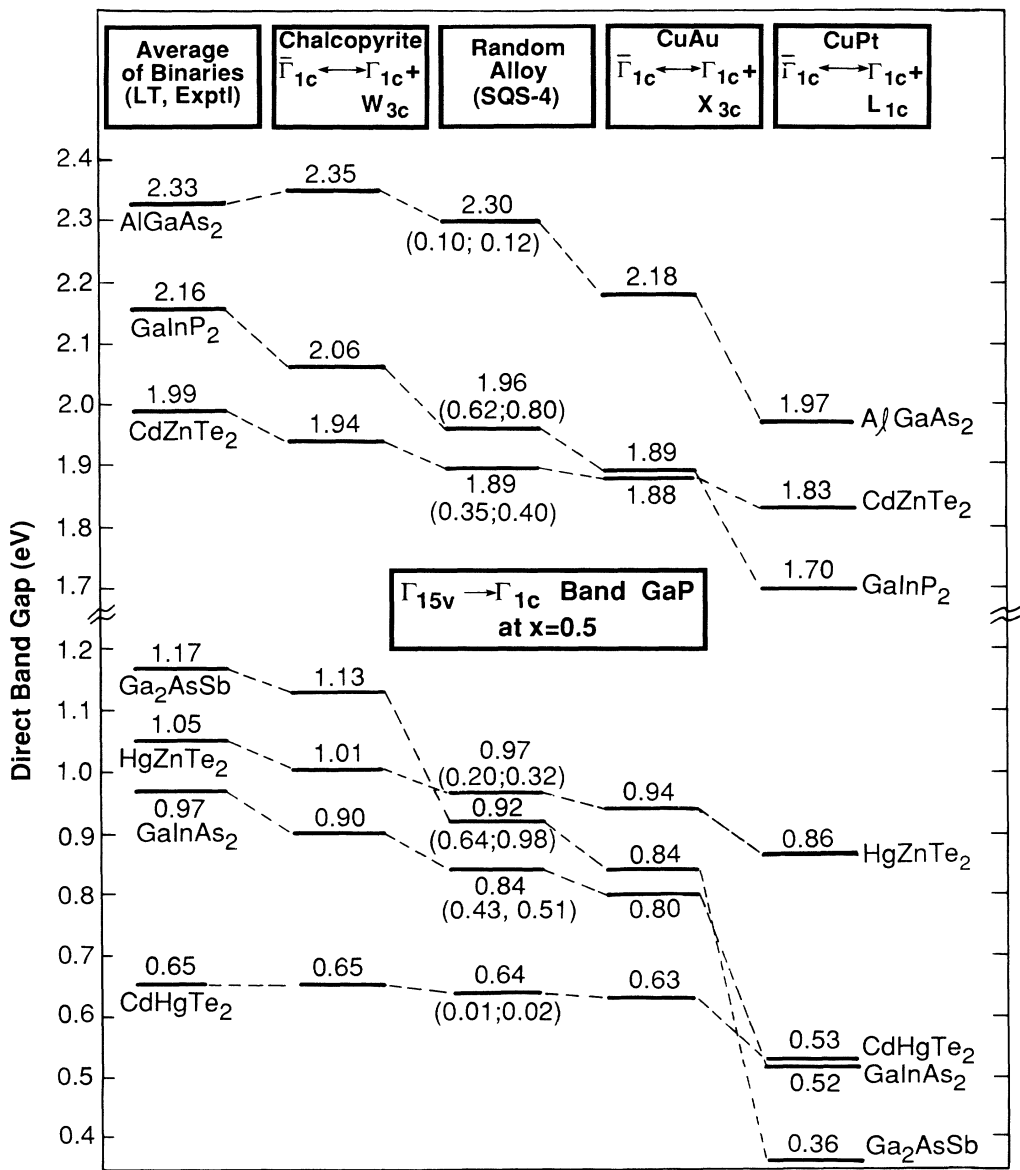


FIG. 13. Predicted direct band gaps $\Gamma_{\text{VBM}} \rightarrow \Gamma_{1c}$ of seven ABC_2 semiconducting system in the CA, CH, CP, and random (SQS-4) structures. The numbers in the parentheses are bowing coefficients for the random alloy with (first number) or without (second number) crystal-field average, respectively.

TABLE XII. The first eight columns give the (LAPW-calculated, unless otherwise noted) direct band gaps at Γ (in eV) at the 50%-50% average volume for seven ordered structures. Application of the cluster expansion to these values gives the effective cluster energies ϵ_f , from which we predict through Eq. (2.7) the direct band gap of SQS-8 and that of the random alloy $E_g(R)$. For the first four alloys we give $E_g(R)$ predicted from $N_s = 5, 6$, and 7 ordered structures, respectively. For $N_s = 5$ we used $A, B, CA, L1, L3$ for structures ($L1$ denotes Cu_3Au and $L3$ denotes $CuAu_3$) and $J_0, J_1, J_{2,1}, J_{3,1}J_{4,1}$ for interactions. For $N_s = 6$ we used the structures $A, B, CA, CH, CP, Z2$, and the interactions $J_0, J_1, J_{2,1}, J_{2,2}J_{2,3}, J_{2,4}$. For $N_s = 7$ we added SQS-4 to the structures and $J_{2,6}$ to the interactions. All the results are averaged over crystal-field splitting at the VBM.

System	Band gaps from direct calculations						Predicted $E_g(R, x = \frac{1}{2})$	Predicted			
	$E_g(A)$	$E_g(B)$	$E_g(CA)$	$E_g(CH)$	$E_g(CP)$	$E_g(Z2)$		$E_g(SQS-8)$	$N=5$	$N=6$	$N=7$
Al-Ga-As	1.85	0.24	0.91	1.07	0.69	0.95	1.02	0.98	0.91	0.93	0.97
Ga-Sb-As	0.63	-0.63	-0.29	-0.04	-0.70	-0.17	-0.16	-0.19	-0.22	-0.26	-0.22
In-Ga-P	0.97	0.54	0.72	0.84	0.54	0.75	0.77	0.76	0.69	0.73	0.74
Ga-As-P ^a	2.18	0.71	1.41	1.42	1.42	1.36	1.40	1.41	1.41	1.40	1.41
In-Ga-As	0.00	-0.61	-0.32	-0.26	-0.60	-0.30	-0.30	-0.32	-0.36	-0.36	-0.33
Cd-Hg-Te	0.47	-0.99	-0.27	-0.24	-0.37	-0.27	-0.26	-0.27	-0.28	-0.28	-0.27
Cd-Zn-Te	0.75	0.59	0.68	0.70	0.62	0.68	0.66	0.67	0.67	0.67	0.67
Hg-Zn-Te	-0.78	0.57	-0.01	-0.02	-0.06	-0.07	-0.04	-0.04	-0.05	-0.05	-0.04

^aPseudopotential calculation.

the band gap $E_g(R)$ of the random alloy at $x = \frac{1}{2}$, despite the fact that the band gaps $E_g(s)$ of the ordered structures used in this expansion cover a wide range of values.

(iii) SQS-8 provides a consistent description of the band gap of the perfectly random alloy, as evidenced by the fact that in the cluster expansion $E_g(SQS-8) \approx E_g(R)$ (Table XII). Furthermore, we notice that $\delta E = E_g(SQS-4) - E_g(R)$ is small and, in general, positive. The discrepancy becomes larger when there is a large crystal-field splitting (e.g., $GaAs_{0.5}Sb_{0.5}$) or when the interband coupling is large (e.g., $Al_{0.5}Ga_{0.5}As$).

TABLE XIII. Cluster-expansion prediction of the direct band gap of $GaAs_{0.5}P_{0.5}$ and $Al_{0.5}Ga_{0.5}As$ in the random structure (R) and SQS- N , obtained with N_s terms in the expansion (2.10) and (2.11). For comparison we give also the directly calculated gaps in SQS-4 and SQS-8 using the pseudopotential (PS) method. Results are averaged over the crystal-field splitting.

	$E_g(R)$	$E_g(SQS-4)$	$E_g(SQS-8)$
$GaAs_{0.5}P_{0.5}$			
Predictions of cluster expansion			
$N_s = 5$	1.41	1.40	1.41
$N_s = 6$	1.40	1.39	1.40
$N_s = 7$	1.41	1.40	1.40
Direct PS		1.40	1.40
$Al_{0.5}Ga_{0.5}As$			
Predictions of cluster expansion			
$N_s = 5$	1.42	1.55	1.42
$N_s = 6$	1.32	1.33	1.34
$N_s = 7$	1.35	1.40	1.37
Direct PS		1.40	1.38

(iv) Among the simple structures considered, the CuAu is the single best two-atom representation of the random alloy. A similar conclusion can be drawn from Table VI showing that the mixing enthalpy of CA (denoted there as SQS-2) best represents the results of the random alloy. This agrees with a similar observation made earlier³⁷ on empirical grounds.

VI. SUMMARY

We have shown that it is possible to design periodic supercells with A and B atoms such that the first few structural correlation functions closely reproduce those in a perfectly random infinite binary alloy. Physical properties that depend primarily on the local atomic structure of the alloy can then be described by applying electronic Hamiltonians to such “special quasirandom structures.” We find that these SQS’s are (i) short-period superlattices in unusual orientations, with (ii) just a few atoms per cell, and with (iii) site symmetries that are distinctly lower than those of the end-point constituent solids A and B . Description of the electronic structure of such SQS’s within the local-density formalism reveals significant atomic relaxations consistent with the lower site symmetry of atoms in the alloy. This leads to (i) substantial lowering of the alloy’s formation enthalpies, (ii) the existence of a bimodal bond length distribution, (iii) weak crystal-field splittings of states degenerate in A or B , (iv) folded (no-phonon) pseudodirect transitions, (v) strong interband mixing, (vi) broadening of the VCA state, (vii) sublattice localization, and (viii) optical bowing of the band gaps. This method, illustrated here for fcc semiconductor alloys at $x = \frac{1}{2}$, can be readily generalized to other compositions, symmetries, and to imperfectly disordered alloys and affords accurate descriptions of electronic, structural, and thermodynamic properties of alloys within any electronic Hamiltonian (pseudopotential, tight-binding, KKR, etc.) without resort to non-structural models such as the VCA or the SCPA.

ACKNOWLEDGMENTS

This work was supported by the Office of Energy Research, Basic Energy Science (OER-BES), Division of Materials Research, under Grant No. DE-AC02-77CH00178. We are particularly grateful for a grant of computer time from OER-BES. One of us (J.E.B.) acknowledges receipt of support from the Directors Development Fund of the Solar Energy Research Institute. We are grateful to A. B. Chen, K. Hass, and P. Turchi for helpful comments on the manuscript.

APPENDIX: STATISTICS FOR RANDOM ALLOYS

AT $x = \frac{1}{2}$

Here we derive some of the basic quantities pertaining to random alloys, i.e., the average correlation functions [Eq. (2.8)], their variances (see Sec. II D), and the average number of neighbors of opposite type [Eq. (3.2)]. We will focus our discussions on the random alloy at $x = \frac{1}{2}$.

A perfectly random alloy is characterized by statistically independent occupations at N sites. The lattice-averaged (denoted by bar) correlation function for pairs ($k=2$) of spins separated by m th-neighbor distance is

$$\bar{\Pi}_m(\sigma) = \frac{1}{2D_m N} \sum_{i,j} \Delta_m(i,j) \hat{S}_i \hat{S}_j , \quad (\text{A1})$$

where \hat{S}_i and \hat{S}_j are spin variables at sites i and j , respectively, taking values -1 (if site is occupied by A) or $+1$ (if occupied by B). Here, $\Delta_m(i,j)$ is 1 if sites i and j are m th-order neighbors, and zero otherwise. The number of pairs of order m per site is

$$D_m = Z_m / 2 , \quad (\text{A2})$$

where Z_m is the number of m th-order neighbors to a site. The sum in Eq. (A1) extends over all N sites.

The ensemble average of Eq. (A1) for a perfectly random alloy is

$$\bar{\Pi}_m(R) = \langle \bar{\Pi}_m \rangle = \frac{1}{2D_m N} \sum_{i,j} \Delta_m(i,j) \langle \hat{S}_i \hat{S}_j \rangle , \quad (\text{A3})$$

where $\langle \hat{S}_i \hat{S}_j \rangle$ is the ensemble-average spin product on two sites. Since for independent spins at $x = \frac{1}{2}$,

$$\langle S_i S_j \rangle = \delta_{ij} \quad (\text{A4})$$

and $\Delta_m(i,i) = 0$, hence

$$\bar{\Pi}_m(R) = 0 . \quad (\text{A5})$$

Since

$$\langle \bar{\Pi}_m^2 \rangle = \frac{1}{4D_m^2 N^2} \sum_{ij} \sum_{kl} \Delta_m(i,j) \Delta_m(k,l) \langle \hat{S}_i \hat{S}_j \hat{S}_k \hat{S}_l \rangle , \quad (\text{A6})$$

and the average of the four-spin product for $i \neq j$ and $k \neq l$ at $x = \frac{1}{2}$ is

$$\langle \hat{S}_i \hat{S}_j \hat{S}_k \hat{S}_l \rangle = \delta_{ik} \delta_{jl} + \delta_{il} \delta_{jk} , \quad (\text{A7})$$

hence

$$\eta_m(N) = (\langle \bar{\Pi}_m^2 \rangle)^{1/2} = (D_m N)^{-1/2} , \quad (\text{A8})$$

as noted in the text (Sec. II D).

Finally, we derive the expressions for the number of opposite atoms in the m th-neighbor shell, relative to an atom at site i . For the random alloy at $x = \frac{1}{2}$ we can assume, without loss of generality, that an atom A ($\hat{S}_i = -1$) lies at $i=0$. Then [denoting $\Delta_m(j) \equiv \Delta_m(0,j)$]

$$O_m = \frac{1}{2} \sum_j \Delta_m(j) (1 + \hat{S}_j) , \quad (\text{A9})$$

where the sum is extended over j alone. The term in parentheses in Eq. (A9) is

$$1 + \hat{S}_j = \begin{cases} 2 & \text{if } \hat{S}_j = 1 \text{ (B atom)}, \\ 0 & \text{if } \hat{S}_j = -1 \text{ (A atom)}. \end{cases} \quad (\text{A10})$$

For the random alloy, the combined ensemble and lattice site average is the same as the ensemble average only, since all the sites are equivalent. At $x = \frac{1}{2}$ this gives

$$\langle O_m \rangle = \frac{1}{2} \sum_j \Delta_m(j) (1 + \langle \hat{S}_j \rangle) = \frac{1}{2} \sum_j \Delta_m(j) = D_m , \quad (\text{A11})$$

where we have used $\langle S_j \rangle = 0$. Since

$$\langle O_m^2 \rangle = \frac{1}{4} \sum_{j,k} \Delta_m(j) \Delta_m(k) \langle 1 + \hat{S}_j + \hat{S}_k + \hat{S}_j \hat{S}_k \rangle , \quad (\text{A12})$$

we have

$$\langle O_m^2 \rangle = D_m^2 + D_m / 2 . \quad (\text{A13})$$

Then the variance $\langle O_m^2 \rangle - \langle O_m \rangle^2$ is just $D_m/2$. Hence the average number of atoms in the m th-neighbor shell of opposite type to the atom at site i is

$$\langle O_m \rangle = D_m \pm \sqrt{D_m / 2} . \quad (\text{A14})$$

This is Eq. (3.2). Some values are given in the last line of Tables IV and V.

¹J. C. Woolley, in *Compound Semiconductors*, edited by R. K. Willardson and H. L. Goering (Reinhold, New York, 1962), p. 3.
²N. K. Abrikosov, V. F. Bankina, L. V. Poretskaya, L. E. Shelimova, and E. V. Skudnova, *Semiconducting II-VI, IV-V, and V-VI Compounds* (Plenum, New York, 1969).

³N. A. Goryunova, *The Chemistry of Diamond-Like Semiconductors* (MIT, Cambridge, 1963).
⁴A. N. Pikhtin, *Fiz. Tekh. Poluprovodn.* **11**, 425 (1977) [Sov. Phys.—Semicond. **11**, 245 (1977)].
⁵S. S. Vishnubhatla, B. Eyglunent, and J. C. Woolley, *Can. J. Phys.* **47**, 1661 (1968).

- ⁶D. Long, in *Semiconductors and Semimetals*, edited by R. K. Willardson and A. C. Beer (Academic, New York, 1966), Vol. 1, p. 143.
- ⁷O. Madelung, *Physics of III-V Compounds* (Wiley, New York, 1964), p. 269.
- ⁸L. Vegard, *Z. Phys.* **5**, 17 (1921).
- ⁹L. Nordheim, *Ann. Phys. (Leipzig)* **9**, 607 (1931).
- ¹⁰P. Soven, *Phys. Rev.* **156**, 809 (1967); D. W. Taylor, *ibid.* **156**, 1017 (1967); U. Onodera and Y. Toyozawa, *J. Phys. Soc. Jpn.* **24**, 341 (1968); B. Velicky, S. Kirkpatrick, and H. Ehrenreich, *Phys. Rev.* **175**, 747 (1968).
- ¹¹J. F. Hunter, G. Ball, and D. J. Morgan, *Phys. Status Solidi B* **45**, 679 (1971).
- ¹²K. R. Schulze, H. Neumann, and K. Unger, *Phys. Status Solidi B* **75**, 493 (1976).
- ¹³A. Baldereschi, E. Hess, K. Maschke, H. Neumann, K. R. Schulze, and K. Unger, *J. Phys. C* **10**, 4709 (1977).
- ¹⁴D. Richardson, *J. Phys. C* **4**, L289 (1971).
- ¹⁵D. Richardson, *J. Phys. C* **4**, L335 (1971).
- ¹⁶R. Hill and D. Richardson, *J. Phys. C* **4**, L339 (1971).
- ¹⁷D. Richardson, *J. Phys. C* **5**, L26 (1972).
- ¹⁸R. Hill, *J. Phys. C* **7**, 521 (1974).
- ¹⁹J. A. Van Vechten and T. K. Bergstresser, *Phys. Rev. B* **1**, 3351 (1970).
- ²⁰D. Richardson and R. Hill, *J. Phys. C* **5**, 821 (1972).
- ²¹T. P. Pearsall, in *GaInAsP Alloy Semiconductors*, edited by T. P. Pearsall (Wiley Interscience, New York, 1982), p. 295.
- ²²A. B. Chen and A. Sher, *Phys. Rev. B* **22**, 3886 (1980).
- ²³W. Porod, D. K. Ferry, and K. A. Jones, *J. Vac. Sci. Technol.* **21**, 965 (1982).
- ²⁴P. A. Fedders and C. W. Myles, *Phys. Rev. B* **29**, 802 (1984).
- ²⁵D. J. Chadi, *Phys. Rev. B* **16**, 790 (1977).
- ²⁶D. Stroud and H. Ehrenreich, *Phys. Rev. B* **2**, 3197 (1970).
- ²⁷A. B. Chen and A. Sher, *Phys. Rev. B* **23**, 5360 (1981).
- ²⁸F. Aymerich, *Phys. Rev. B* **26**, 1968 (1982); **28**, 6071 (1983).
- ²⁹E. Sigga, *Phys. Rev. B* **10**, 5147 (1974).
- ³⁰D. Z. Y. Ting and Y. C. Chang, *Phys. Rev. B* **30**, 3309 (1984).
- ³¹K. C. Hass, E. Ehrenreich, and B. Velicky, *Phys. Rev. B* **27**, 1088 (1983).
- ³²H. Ehrenreich and K. C. Hass, *J. Vac. Sci. Technol.* **21**, 133 (1982).
- ³³A. B. Chen and A. Sher, *Phys. Rev. B* **17**, 4726 (1978).
- ³⁴S. Sakai and T. Sugano, *J. Appl. Phys.* **50**, 4143 (1979).
- ³⁵G. M. Stocks and H. Winter, in *The Electronic Structure of Complex Systems*, Vol. 113 of *NATO Advanced Study Institute Series B: Physics*, edited by P. Phariseau and W. M. Temmerman (Plenum Press, New York, 1984), p. 463.
- ³⁶J. S. Faulkner, *Prog. Mater. Sci.* **27**, 1 (1982).
- ³⁷(a) J. E. Bernard and A. Zunger, *Phys. Rev. B* **36**, 3199 (1987); **34**, 5992 (1986); (b) S.-H. Wei and A. Zunger, *Phys. Rev. B* **39**, 3279 (1989); (c) S.-H. Wei and A. Zunger, *J. Vac. Sci. Technol. A* **6**, 2597 (1988).
- ³⁸S. M. Kelso, D. E. Aspnes, M. A. Pollack, and R. N. Nahory, *Phys. Rev. B* **26**, 6669 (1982).
- ³⁹A. B. Chen and A. Sher, *Phys. Rev. Lett.* **40**, 900 (1978).
- ⁴⁰(a) W. E. Spicer, J. A. Silberman, J. Morgan, I. Lindau, J. A. Wilson, A. B. Chen, and A. Sher, *Phys. Rev. Lett.* **49**, 948 (1982); *Physica* **117&118B**, 60 (1983); (b) K. L. Tsang, J. E. Rowe, T. A. Calleott, and R. A. Logan, *Phys. Rev. B* **38**, 13 277 (1988); (c) K. C. Hass, *Phys. Rev. B* **40**, 5780 (1989).
- ⁴¹See numerous references in *Redistribution Reactions*, by J. C. Lockhart (Academic, New York, 1970).
- ⁴²(a) J. C. Mikkelsen and J. B. Boyce, *Phys. Rev. Lett.* **49**, 1412 (1982); *Phys. Rev. B* **28**, 7130 (1983); J. B. Boyce and J. C. Mikkelsen, *Phys. Rev. B* **31**, 6903 (1985); (b) J. B. Boyce and J. C. Mikkelsen, in *Ternary and Multinary Compounds*, edited by S. K. Deb and A. Zunger (Materials Research Society, Pittsburgh, 1987), p. 359.
- ⁴³A. Balzarotti, N. Motta, M. Czyzyk, A. Kissiel, M. Podgorny, and M. Zimnal-Starnawska, *Phys. Rev. B* **30**, 2295 (1984); A. Balzarotti, *Physica* **146B**, 150 (1987); A. Balzarotti, N. Motta, A. Kissiel, M. Zimnal-Starnawska, M. T. Czyzyk, and M. Podgorny, *Phys. Rev. B* **31**, 7526 (1985).
- ⁴⁴B. A. Bunker, *J. Vac. Sci. Technol. A* **5**, 3003 (1987); Q. T. Islam and B. A. Bunker, *Phys. Rev. Lett.* **59**, 2701 (1987).
- ⁴⁵T. Sasaki, T. Onda, R. Ito, and N. Ogasawara, *Jpn. J. Appl. Phys.* **25**, 231 (1986).
- ⁴⁶H. Oyanagi, Y. Takeda, T. Matsushita, T. Ishiguro, and A. Sasaki, *J. Phys. (Paris) Colloq.* **8**, C8-423 (1986); *Superlatt. Microstruct.* **4**, 413 (1988).
- ⁴⁷J. L. Martins and A. Zunger, *Phys. Rev. B* **30**, 6217 (1984).
- ⁴⁸G. P. Srivastava, J. L. Martins, and A. Zunger, *Phys. Rev. B* **31**, 3561 (1985).
- ⁴⁹P. Letardi, N. Motta, and A. Balzarotti, *J. Phys. C* **20**, 2583 (1987).
- ⁵⁰M. Ichimura and A. Sasaki, *J. Electron. Mater.* **17**, 305 (1988); *Phys. Rev. B* **36**, 9694 (1987); *J. Appl. Phys.* **60**, 3850 (1986); *Jpn. J. Appl. Phys.* **26**, 246 (1987); **26**, 1296 (1987).
- ⁵¹R. Weil, R. Nkum, E. Muranovich, and L. Benguigui, *Phys. Rev. Lett.* **62**, 2744 (1989).
- ⁵²A. Mbaye, L. G. Ferreira, and A. Zunger, *Phys. Rev. Lett.* **58**, 49 (1987).
- ⁵³L. G. Ferreira, A. Mbaye, and A. Zunger, *Phys. Rev. B* **35**, 6475 (1987); **37**, 10 547 (1988).
- ⁵⁴(a) A. Mbaye, D. M. Wood, and A. Zunger, *Phys. Rev. B* **37**, 3008 (1988); (b) D. M. Wood and A. Zunger, *Phys. Rev. Lett.* **61**, 1501 (1988).
- ⁵⁵(a) L. G. Ferreira, S.-H. Wei, and A. Zunger, *Phys. Rev. B* **40**, 3197 (1989); (b) S.-H. Wei, L. G. Ferreira, and A. Zunger, *Phys. Rev. B* **41**, 8240 (1990); (c) A. E. Carlsson, *Phys. Rev. B* **35**, 4858 (1987).
- ⁵⁶S.-H. Wei, A. Mbaye, L. G. Ferreira, and A. Zunger, *Phys. Rev. B* **36**, 4163 (1987); A. Zunger, S.-H. Wei, A. Mbaye, and L. G. Ferreira, *Acta Metall.* **36**, 2239 (1988).
- ⁵⁷K. Beshtah, D. Zamir, P. Becla, P. A. Wolff, and R. G. Griffin, *Phys. Rev. B* **36**, 6420 (1987).
- ⁵⁸D. B. Zax, S. Vega, N. Yellin, and D. Zamir, *Chem. Phys. Lett.* **130**, 105 (1987).
- ⁵⁹A. Kobayashi and A. Roy, *Phys. Rev. B* **35**, 5611 (1987).
- ⁶⁰R. Carles, G. Landa, and J. B. Renucci, *Solid State Commun.* **53**, 179 (1985).
- ⁶¹P. J. Dean, G. Kaminsky, and R. B. Zetterstrom, *Phys. Rev. B* **181**, 1149 (1969); B. L. Joesten and F. C. Brown, *ibid.* **148**, 919 (1986).
- ⁶²A. Bieber and F. Gautier, *Physica* **107B**, 71 (1981).
- ⁶³K. C. Hass, R. J. Lempert, and H. Ehrenreich, *Phys. Rev. Lett.* **52**, 77 (1984); R. J. Lempert, K. C. Hass, and H. Ehrenreich, *Phys. Rev. B* **36**, 1111 (1987); F. Ducastelle, *J. Phys. (Paris) Colloq.* **33**, C3-269 (1972); F. Brouers and F. Ducastelle, *J. Phys. F* **5**, 45 (1975); F. Cyrot-Lackman and F. Ducastelle, *Phys. Rev. Lett.* **27**, 429 (1971); F. Brouers, F. Ducastelle, F. Gautier, and J. van der Rest, *J. Phys. (Paris) Colloq.* **35**, C4-89 (1974).
- ⁶⁴R. Mills and P. Ratanavararaka, *Phys. Rev. B* **18**, 5291 (1978).
- ⁶⁵T. Kaplan and P. L. Leath, L. J. Gray, and H. W. Diehl, *Phys. Rev. B* **21**, 4230 (1980).
- ⁶⁶A. Zin and E. A. Stern, *Phys. Rev. B* **31**, 4954 (1985); E. A. Stern and A. Zin, *ibid.* **9**, 1170 (1974).

- ⁶⁷*Local Density Approximations in Quantum Chemistry and Solid State Physics*, edited by J. P. Dahl and J. Avery (Plenum, New York, 1984).
- ⁶⁸*The Electronic Structure of Complex Systems*, Vol. 113 of *NATO Advanced Study Institute, Series B: Physics*, edited by P. Phariseau and W. M. Temmerman (Plenum, New York, 1982).
- ⁶⁹*Electronic Structure, Dynamics and Quantum Structural Properties of Condensed Matter*, Vol. 121 of *NATO Advanced Study Institute, Series B: Physics*, edited by J. T. Devreese and P. VanCamp (Plenum, New York, 1984).
- ⁷⁰A preliminary report of this work was described in A. Zunger, S.-H. Wei, L. G. Ferreira, and J. E. Bernard, *Phys. Rev. Lett.* **65**, 353 (1990). Results using the SQS were previously reported by S.-H. Wei and A. Zunger, *Appl. Phys. Lett.* **56**, 662 (1990).
- ⁷¹C. M. Van Baal, *Physica (Utrecht)* **64**, 571 (1973).
- ⁷²R. Kikuchi, *Phys. Rev.* **81**, 988 (1951).
- ⁷³T. Morita, *J. Phys. Soc. Jpn.* **12**, 753 (1957).
- ⁷⁴J. M. Sanchez, F. Ducastelle, and D. Gratias, *Physica A* **128**, 334 (1984).
- ⁷⁵C. Domb, in *Phase Transitions and Critical Phenomena*, edited by C. Domb and M. S. Green (Academic, London, 1974), Vol. 3, p. 357.
- ⁷⁶D. de Fontaine, in *Solid State Physics*, edited by H. Ehrenreich, F. Seitz, and D. Turnbull (Academic, New York, 1979), Vol. 34, p. 73.
- ⁷⁷D. J. Chadi and M. L. Cohen, *Phys. Rev. B* **8**, 5747 (1973); S. Frojen, *Phys. Rev. B* **39**, 3168 (1989).
- ⁷⁸P. Hohenberg and W. Kohn, *Phys. Rev.* **136**, 864 (1964); W. Kohn and L. J. Sham, *ibid.* **140**, 1133 (1965).
- ⁷⁹J. Ihm, A. Zunger, and M. L. Cohen, *J. Phys. C* **12**, 4409 (1979).
- ⁸⁰P. Bendt and A. Zunger, *Phys. Rev. Lett.* **50**, 1684 (1983).
- ⁸¹O. H. Nielsen and R. M. Martin, *Phys. Rev. B* **32**, 3780 (1985).
- ⁸²S.-H. Wei and H. Krakauer, *Phys. Rev. Lett.* **55**, 1200 (1985), and references therein.
- ⁸³D. Ceperley and B. J. Alder, *Phys. Rev. Lett.* **45**, 566 (1980); J. P. Perdew and A. Zunger, *Phys. Rev. B* **23**, 5048 (1981).
- ⁸⁴K. Binder, *Phys. Rev. Lett.* **45**, 811 (1980); K. Binder, J. L. Lebowitz, M. K. Phani, and M. H. Kalos, *Acta Metall.* **29**, 1655 (1981). See also *Application of Monte-Carlo Method in Statistical Physics*, 2nd ed., edited by K. Binder (Springer-Verlag, Berlin, 1989).
- ⁸⁵S. Lee, D. M. Bylander, and L. Kleinman, *Phys. Rev. B* **40**, 8399 (1989).
- ⁸⁶L. C. Davis, *Phys. Rev. B* **28**, 6961 (1983).
- ⁸⁷L. C. Davis and H. Holloway, *Solid State Commun.* **64**, 121 (1987).
- ⁸⁸R. Alben, M. Blume, H. Krakauer, and L. Schwartz, *Phys. Rev. B* **12**, 4090 (1975); J. J. Rehr and R. Alben, *ibid.* **16**, 2400 (1977); R. Alben, M. Blume and M. McKewon, *ibid.* **16**, 3829 (1977).
- ⁸⁹D. Henderson and J. B. Ortenburger, *J. Phys. C* **6**, 631 (1973).
- ⁹⁰Ph. Lambin and J. P. Gaspard, *J. Phys. F* **10**, 651 (1980); **10**, 2413 (1980).
- ⁹¹M. Weissmann and N. V. Cohan, *J. Phys. C* **8**, 109 (1975); **9**, 473 (1976); N. V. Cohan, C. A. Efeyan, and M. Weissmann, *ibid.* **9**, L679 (1976).
- ⁹²(a) A. Berera, H. Dreysse, L. T. Wille, and D. de Fontaine, *J. Phys. F* **18**, L49 (1988); (b) H. Dreysse, A. Berera, L. T. Wille, and D. de Fontaine, *Phys. Rev. B* **39**, 2442 (1989).
- ⁹³J. P. Gaspard and F. Cyrot-Lackmann, *J. Phys. C* **6**, 3077 (1973).
- ⁹⁴P. S. Julienne and S. Choi, *J. Chem. Phys.* **53**, 2726 (1970).
- ⁹⁵J. W. D. Connolly and A. R. Williams, *Phys. Rev. B* **27**, 5169 (1983).
- ⁹⁶W. H. Butler and W. Kohn, *J. Res. Natl. Bur. Stand.* **74A**, 443 (1970).
- ⁹⁷K. Terakura, T. Oguchi, T. Mohri, and K. Watanabe, *Phys. Rev. B* **35**, 2169 (1987); S. Takizawa and K. Terakura, *ibid.* **39**, 5792 (1989).
- ⁹⁸M. F. Ling and D. J. Miller, *Phys. Rev.* **34**, 7388 (1986); **38**, 6113 (1988).
- ⁹⁹S. H. Wei and A. Zunger, *Phys. Rev. B* **39**, 6279 (1989).
- ¹⁰⁰In Ref. 85, Lee, Bylander, and Kleinman adopted a slightly different random sampling method. To assure that the sample composition is exactly $x = \frac{1}{2}$ (rather than that the average over many attempts is $\frac{1}{2}$), they assigned a random number to each of the N sites and another set of random numbers to each of the $N/2$ A and $N/2$ B atoms. The sites and the atoms were then listed in order of increasing random number and paired off. We find that this method reduces the standard deviation $\eta_{k,m}(N)$ relative to the regular random sampling. However, the average of the correlation functions over many such attempts is no longer zero (as in the regular sampling method). For $\bar{\Pi}_{2,1}$ it is ~ -0.14 for $N=8$, ~ -0.067 for $N=16$, and ~ -0.033 for $N=32$.
- ¹⁰¹G. Kerker, *J. Phys. C* **13**, L189 (1980).
- ¹⁰²P. N. Keating, *Phys. Rev.* **145**, 637 (1966).
- ¹⁰³R. G. Dandrea, J. E. Bernard, S.-H. Wei, and A. Zunger, *Phys. Rev. Lett.* **64**, 36 (1990).
- ¹⁰⁴J. E. Bernard, S.-H. Wei, D. M. Wood, and Z. Zunger, *Appl. Phys. Lett.* **52**, 311 (1988); S.-H. Wei and A. Zunger, *J. Appl. Phys.* **63**, 5794 (1988).
- ¹⁰⁵J. J. Hopfield, *J. Phys. Chem. Solids* **15**, 97 (1960).
- ¹⁰⁶J. A. Van Vechten, O. Berolo, and J. C. Woolley, *Phys. Rev. Lett.* **29**, 1400 (1972).
- ¹⁰⁷*Numerical Data and Functional Relationships in Science and Technology*, Group III, Vols. 17a and 17b of *Landolt-Börnstein New Series*, edited by O. Madelung, M. Schulz, and H. Weiss (Springer-Verlag, Berlin, 1982). See also Ref. 37.
- ¹⁰⁸J. E. Bernard, L. G. Ferreira, S.-H. Wei, and A. Zunger, *Phys. Rev. B* **38**, 6338 (1988).
- ¹⁰⁹S. Frojen and A. Zunger (unpublished).
- ¹¹⁰A. Gomyo, T. Suzuki, and S. Iijima, *Phys. Rev. Lett.* **60**, 2645 (1988).
- ¹¹¹H. R. Jen, M. J. Cherng, and G. B. Stringfellow, *Appl. Phys. Lett.* **48**, 1603 (1986).
- ¹¹²T. S. Kuan, W. I. Wang, and E. L. Wilkie, *Appl. Phys. Lett.* **51**, 51 (1987); T. Fukui and H. Saito, *Jpn. J. Appl. Phys.* **23**, L521 (1984).
- ¹¹³K. C. Hass, L. C. Davis, and A. Zunger, *Phys. Rev. B* **42**, 3757 (1990).

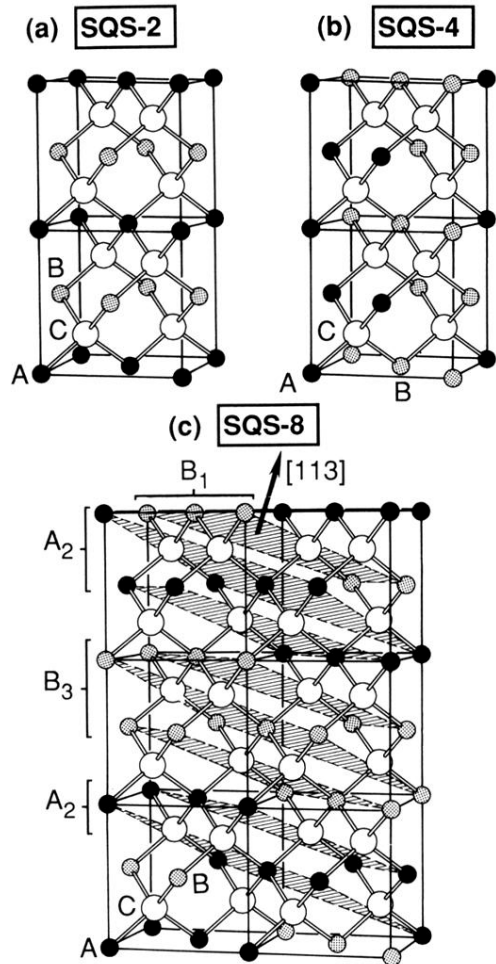


FIG. 1. Crystal structure of three special quasirandom structure. (a) SQS-2 is a (1,1) superlattice in the [001] direction; (b) SQS-4 is a (2,2) superlattice in the [110] direction; and (c) SQS-8 is a (2,3,2,1) superlattice in the [113] direction. The (113) planes are shaded in (c), and the stacking arrangement is indicated.